LETTERS
https://doi.org/10.1038/s41564-019-0579-2
nature microbiology

Breakdown of *Vibrio cholerae* biofilm architecture induced by antibiotics disrupts community barrier function

Francisco Díaz-Pascual[1], Raimo Hartmann[1], Martin Lempp[1], Lucia Vidakovic[1], Boya Song[2], Hannah Jeckel[1,3], Kai M. Thormann[4], Fitnat H. Yildiz[5], Jörn Dunkel[2], Hannes Link[1,6], Carey D. Nadell[1,7] and Knut Drescher[1,3,6*]

Bacterial cells in nature are frequently exposed to changes in their chemical environment[1,2]. The response mechanisms of isolated cells to such stimuli have been investigated in great detail. By contrast, little is known about the emergent multicellular responses to environmental changes, such as antibiotic exposure[3–7], which may hold the key to understanding the structure and functions of the most common type of bacterial communities: biofilms. Here, by monitoring all individual cells in *Vibrio cholerae* biofilms during exposure to antibiotics that are commonly administered for cholera infections, we found that translational inhibitors cause strong effects on cell size and shape, as well as biofilm architectural properties. We identified that single-cell-level responses result from the metabolic consequences of inhibition of protein synthesis and that the community-level responses result from an interplay of matrix composition, matrix dissociation and mechanical interactions between cells. We further observed that the antibiotic-induced changes in biofilm architecture have substantial effects on biofilm population dynamics and community assembly by enabling invasion of biofilms by bacteriophages and intruder cells of different species. These mechanistic causes and ecological consequences of biofilm exposure to antibiotics are an important step towards understanding collective bacterial responses to environmental changes, with implications for the effects of antimicrobial therapy on the ecological succession of biofilm communities.

Exposure to antibiotics is an important stimulus for bacteria, and is likely to be ubiquitous inside patients receiving antibiotic therapy as well as in the broader environment, where biofilm formation and antibiotic-mediated microbial warfare are common[3–7]. Understanding community-scale effects of antibiotic treatment in biofilms is important, given that antibiotic-tolerant infections are currently among the largest emerging global health threats[8–15], in part due to the increased tolerance of biofilms to antibiotics[16–24].

To investigate the emergent community-level responses of antibiotic exposure on biofilm populations, we subjected mature *V. cholerae* biofilms to antibiotics encompassing the major mechanisms of action (Extended Data Fig. 1), including the most commonly used antibiotic classes against cholera infections[25]. Our recently developed single-cell imaging system for biofilm dynamics[26–28] enabled us to detect architectural changes of biofilms in response to antibiotic treatment above the minimum inhibitory concentration (MIC), which were particularly striking for translational inhibitors such as tetracycline (Fig. 1a–c and Extended Data Fig. 1). We observed modifications in cell morphology and biofilm architecture during tetracycline treatment for several parameters, including marked changes in both the cell volume and cell-packing density (Fig. 1, Extended Data Fig. 2 and Supplementary Videos 1 and 2). Without single-cell-level imaging of biofilms, the expansion of biofilm size caused by antibiotic treatment above the MIC (Fig. 1) would probably have been misinterpreted as antibiotic-induced biofilm formation (see data from classical crystal violet assays in Extended Data Fig. 3 for tetracycline and other antibiotics). To investigate the detailed mechanisms and ecological consequences of antibiotic-induced biofilm architectural changes, unless indicated otherwise, experiments were performed with tetracycline, an antibiotic that is commonly used to treat cholera infections[25].

Modifications to the biofilm architecture appeared within the first 6 h of tetracycline exposure, well before the time at which significant cell death became evident (>10 h; Extended Data Fig. 4), indicating that other processes were reorganizing the biofilms during inhibition of protein translation. After 6 h of tetracycline treatment, cells within biofilms increased in volume by 2.5-fold on average, and the mean cell density decreased by 29% (Fig. 1d). The cell volume increase and the timing of this increase, did not depend on the cellular location within the biofilm (Fig. 1e–h), indicating that tetracycline diffuses into all regions of the biofilm quickly, on a shorter time scale than that of the physiological response to translational inhibition.

While the observed decrease in cell density is an alteration of the multicellular arrangement within the biofilm, the increase in cell volume is a single-cell-level alteration that could potentially also occur outside the biofilm state following tetracycline exposure. To test whether similar changes in cell shape also occur during tetracycline treatment outside biofilms, we treated single cells attached to glass and planktonic cells grown in liquid culture, and observed that these individual cells also increased in volume (Fig. 2a and

[1]Max Planck Institute for Terrestrial Microbiology, Marburg, Germany. [2]Department of Mathematics, Massachusetts Institute of Technology, Cambridge, MA, USA. [3]Department of Physics, Philipps-Universität Marburg, Marburg, Germany. [4]Institut für Mikrobiologie und Molekularbiologie, Justus-Liebig-Universität Gießen, Gießen, Germany. [5]Department of Microbiology and Environmental Toxicology, University of California, Santa Cruz, Santa Cruz, CA, USA. [6]Synmikro Center for Synthetic Microbiology, Philipps-Universität Marburg, Marburg, Germany. [7]Department of Biological Sciences, Dartmouth College, Hanover, USA. *e-mail: k.drescher@mpi-marburg.mpg.de

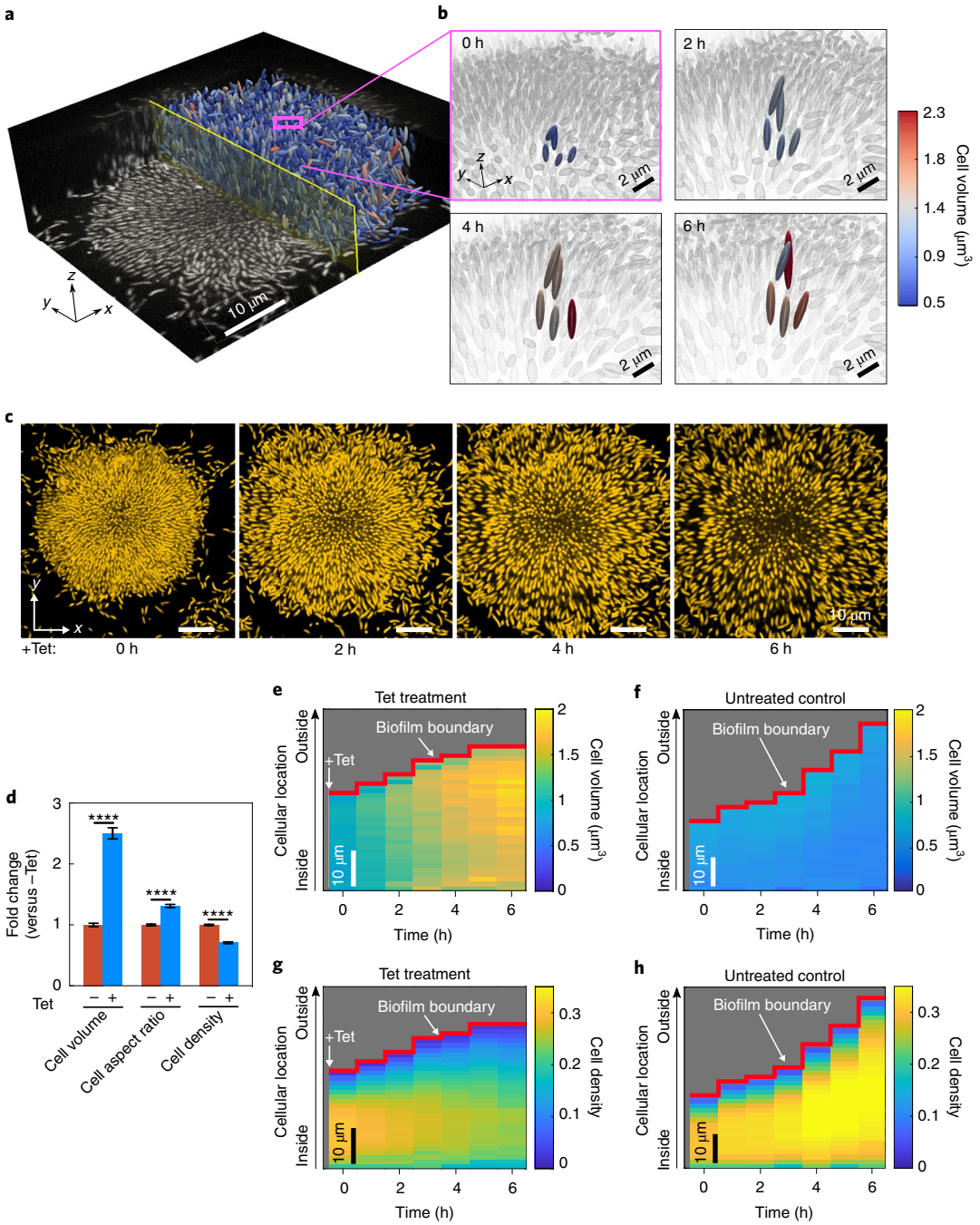

Fig. 1 | Inhibition of protein synthesis triggers strong architectural changes of biofilms. a, Raw microscopy image based on mKOκ fluorescence of a 24-h-old biofilm and 3D visualization of cells as ellipsoids after segmentation, separated by a central plane with a yellow outline. **b**, The box outlined in pink in **a** is enlarged in the four images, showing five cells, which are tracked in 3D during 6 h of tetracycline treatment above the MIC. These five cells are coloured according to their volume and all other cells in the background are coloured grey. Tetracycline treatment results in increased cell volume and decreased cell density (volume fraction). **c**, Snapshots of biofilm architecture dynamics (showing only one confocal *xy* slice located 2 µm above the coverslip) during a tetracycline (Tet)-treatment time series. See also Supplementary Video 1. Cells are visualized using a constitutively expressed mKOκ fluorescent protein. **d**, Fold change of cell volume, cell aspect ratio and cell density (measured as volume fraction) of tetracycline-treated biofilms compared with untreated biofilms grown for the same time without antibiotics. Data are mean ± s.e.m. ($n = 15$ samples for −Tet and $n = 9$ for +Tet; each sample corresponds to a different biofilm). Statistical significance was calculated in relation to control biofilms using a two-sided unpaired *t*-test (****$P < 0.0001$). **e**–**h**, Spatiotemporal changes of the average cell volume with tetracycline treatment (**e**) or for untreated control (**f**) and cell density with tetracycline treatment (**g**) or for untreated control (**h**) as a function of time during tetracycline treatment and position inside the biofilm. Each pixel in these heat maps is coloured according to the average cell volume or cell density at a given time and spatial position in the biofilm. Cell volumes and cell density values are averaged over all cells with similar distances from the interface of the biofilm and the growth medium (that is, the biofilm boundary). Heat maps are representative of $n = 5$ different biofilms.

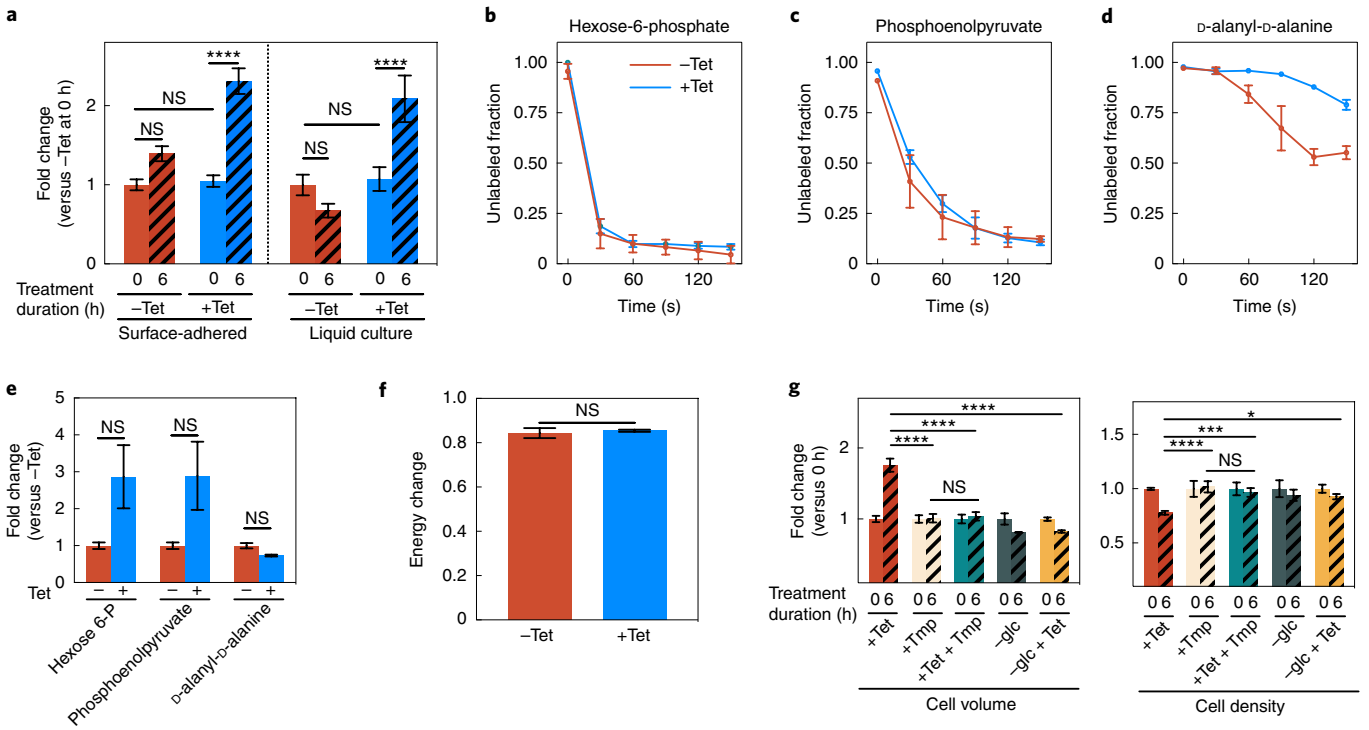

Fig. 2 | Continued metabolic activity of tetracycline-treated cells results during expansion of cell volume. a, Fold change of cell volume of surface-attached isolated cells grown in a microfluidic device and planktonic cells grown in liquid culture with or without tetracycline treatment, normalized to the untreated cell volume at 0 h. Data are mean ± s.e.m., $n = 3$ independent biological replicates. **b**–**d**, Tetracycline-treated cells are metabolically active, as shown by unlabelled ratios of hexose-6-phosphate (the first intermediate of glycolysis) (**b**), phosphoenolpyruvate (late glycolysis intermediate) (**c**) and D-alanyl-D-alanine (cell wall precursor) (**d**). Cells treated for 2 h with tetracycline (blue) or untreated control cells (red) were washed with C^{13}-labelled medium for different times, ranging from 0–150 s (mean ± s.d., $n = 3$ independent biological replicates). **e**, Fold change in hexose-6-phosphate, phosphoenolpyruvate and D-alanyl-D-alanine concentration between tetracycline-treated and untreated cells (mean ± s.e.m., $n = 3$ independent biological replicates). **f**, Energy charge, calculated using ([ATP] + 0.5[ADP])/([ATP] + [ADP] + [AMP]), of tetracycline-treated and control cells (mean ± s.e.m., $n = 3$ independent biological replicates). **g**, Fold changes in cell volume and cell density (measured as volume fraction) of biofilms treated with tetracycline, trimethoprim (Tmp) or tetracycline and Tmp, and with glucose removal (−glc) or glucose removal and tetracycline treatment (−glc + Tet). Data are mean ± s.e.m. Sample sizes (n) are 17 (Tet only), 5 (Tmp only), 6 (Tet + Tmp), 3 (−glc) and 4 (−glc + Tet); each sample corresponds to a different biofilm. For each treatment, the fold change is calculated in relation to the 0 h treatment. In **a** and **g**, statistical significance was calculated using one-way analysis of variance (ANOVA) with Bonferroni's correction for multiple comparisons. In **e** and **f**, statistical significance was calculated using a two-sided unpaired t-test. Statistically non-significant differences (NS) in **a**: $P = 0.067$, 0.99, 0.24 and 0.78 (left to right); in **e**: $P = 0.076$, 0.071 and 0.99 (left to right); in **f**: $P = 0.70$; and in **g**: $P = 0.99$. $^{*}P < 0.05$, $^{***}P < 0.001$ and $^{****}P < 0.0001$.

Extended Data Fig. 5a). We next sought to understand the underlying causes of this increase in cell volume.

To test whether tetracycline-treated cells increase in volume passively due to osmotic effects or actively due to a specific response, we first investigated whether the cells remain metabolically active and continue to produce new cell wall components during tetracycline exposure. We followed the incorporation of ^{13}C-labelled glucose into hexose-6-phosphate metabolites (such as glucose-6-phosphate; upper glycolysis, Fig. 2b), phosphoenolpyruvate (lower glycolysis, Fig. 2c), and the cell wall precursor D-alanyl-D-alanine (Fig. 2d). Labelling of both glycolysis metabolites was almost identical with or without tetracycline treatment and their absolute concentrations were higher in tetracycline-treated cells (Fig. 2e; for fold-changes of 57 other metabolites, see Extended Data Fig. 5b). This indicates that tetracycline-treated cells remain metabolically active and that they catabolize glucose with at least the same rate compared with untreated cells. Cell wall precursors were also continuously produced after tetracycline-treatment, as indicated by the isotope label in D-alanyl-D-alanine (Fig. 2d). The cellular energy state remained unchanged between the tetracycline-treated and untreated cells (Fig. 2f). Despite their high metabolic activity and production of cell wall, tetracycline-treated cells do not divide, as they cannot synthesize new divisome proteins[29]. If there was a causal connection between metabolic activity and cell volume increase, we would expect that the simultaneous inhibition of biosynthetic pathways and protein synthesis would stop the cell volume increase. Indeed, exposing biofilms to the folate-biosynthesis inhibitor trimethoprim abolished the increase in cell volume during tetracycline treatment (Fig. 2g). Similarly, cells for which glucose was removed at the same time that tetracycline was added did not increase in volume. Together, these experiments show that continued metabolic activity without cell division is necessary for the observed increase in cell volume.

Of note, biofilms treated with both trimethoprim and tetracycline together also did not display a change in cell packing density (Fig. 2g), suggesting that the cell volume increase is necessary for the decrease in cell density in the wild-type *V. cholerae*. Applying tetracycline treatment to biofilms at the same time as removing glucose from the medium yielded results identical to those of trimethoprim treatments (Fig. 2g). These results imply that the observed decrease in cell density during tetracycline treatment cannot be caused by a chemical interaction between tetracycline and the biofilm matrix or by an effect of tetracycline on the activity of enzymes that are present at the time of the antibiotic exposure. What then causes the decreased cell density following tetracycline treatment?

The cell packing density in biofilms is probably determined by the local biofilm matrix composition and structure[11,28,30]. By tracking nanometre-sized beads embedded in the matrix during tetracycline treatment, we observed that the matrix was sheared during the decrease in cell density (Fig. 3a), indicating substantial rearrangements of the matrix. To test whether particular matrix components have an effect on the cell density decrease, we investigated deletion mutants of the known *V. cholerae* matrix proteins RbmA, RbmC and Bap1 (ref. [31]). Only Δ*rbmA* biofilms displayed a different phenotype from the wild-type: even though Δ*rbmA* cells in mature biofilms showed a similar increase in cell volume with tetracycline treatment, they did not show a strong decrease in cell density (Fig. 3b), probably because the untreated biofilms already displayed a low initial cell density. This result suggests that the architectural role of RbmA in wild-type biofilms is connected to the decrease in cell density during tetracycline treatment. RbmA has recently been shown to assume one of two conformational states, open or closed; the open state is associated with binding neighbouring cells together[32]. The amino acid substitutions D97A or D97K lock RbmA in the open state, whereas R234A locks RbmA in the closed state[32]. Only biofilms composed of cells with RbmA locked in the open state exhibit a similar biofilm architecture to the wild type, with a decrease in cell density during tetracycline treatment (Fig. 3c), indicating that RbmA-dependent cell–cell binding is important for the tetracycline-induced changes in biofilm cell density.

Using immunostaining to visualize RbmA localization, we found that during tetracycline treatment, gaps emerge between cells and the surrounding matrix material (Fig. 3d and Extended Data Fig. 6), indicating detachment of cells from RbmA. Quantitative immunofluorescence clearly shows that the RbmA levels surrounding each cell decrease rapidly following antibiotic treatment, in contrast to the untreated control (Fig. 3e). To further dissect how RbmA is linked to cell density decreases during tetracycline treatment, we used an inducible-RbmA construct in a Δ*rbmA* background to vary the amount of RbmA produced during biofilm growth before tetracycline exposure. In the absence of antibiotic treatment, the average cell density increased with increasing RbmA concentration (Fig. 3f and Extended Data Fig. 7). Notably, we observed that during tetracycline treatment, the relationship between RbmA concentration and the decrease in cell density has a pronounced minimum (Fig. 3g). This suggests that the number of RbmA-mediated cell–cell bonds in the biofilm before tetracycline exposure could be the key to understanding the cause of the change in cell density during tetracycline exposure.

We hypothesized that the detachment of cells from the matrix and each other is due to breakdown of matrix components. However, deletion of known RbmA-processing proteases (HapA, PrtV and IvaP[33]) had no effect on cell density (Fig. 3i). Nevertheless, RbmA has been shown to bind to the polysaccharide component of the matrix, *Vibrio* polysaccharide (VPS)[32,33], presumably acting as a crosslinker for the VPS matrix. This suggests that the RbmA-mediated adhesion between cells can be affected by cleaving VPS. To test this hypothesis, we exposed biofilms that lack the putative VPS-degrading polysaccharide hydrolase RbmB[34] to tetracycline. In contrast to biofilms composed of wild-type cells, Δ*rbmB* biofilms barely decreased in cell density during tetracycline treatment (Fig. 3i), indicating that the RbmB is necessary for the decreased cell density that is observed in the wild-type. However, wild-type RbmB levels are not sufficient to cause a decrease in cell density without a simultaneous increase in cell volume, as reflected in our trimethoprim and glucose-removal experiments in which the *rbmB* locus was intact (Fig. 2g). Overexpression of *rbmB* decreased the cell density—similar to what was observed after tetracycline treatment (Fig. 3j)—without requiring a change in cell volume. This shows that when present at high levels, the activity of RbmB is sufficient to alter cell density, but at wild-type RbmB levels, RbmB activity must be accompanied by an increase in cell volume to cause the dissociation of the cells from the matrix, presumably because an increase in cell volume with a simultaneous absence of protein synthesis results in a dilution of the number of cell–RbmA bonds per cell surface area.

For several species, it has been shown that the pressure generated by growth-induced expansion of biovolume within biofilms is counteracted by the adhesion of the matrix, resulting in a net compression[35]. Microscopically, this is achieved by a balance between attractive and repulsive interactions between cells[28]. For *V. cholerae*, cell–cell attraction is primarily mediated by RbmA, whereas cell–cell repulsion is mediated by osmotic effects and the secretion of

Fig. 3 | Antibiotic-induced architectural breakdown of biofilms. a, Matrix movement during antibiotic treatment is visualized by fluorescent beads attached to the matrix. Cells expressing the sfGFP fluorescent protein (cyan) were grown in medium containing fluorescent beads diameter 0.1 μm in diameter (red). Occasionally, beads incorporated into the biofilm matrix. During tetracycline treatment, no new beads entered the biofilm. The magnified inset shows the separation of the red bead cluster during tetracycline treatment, revealing differential movement in the matrix. Images are representative of $n=3$ different biofilms. **b**, Cell volume and cell density (measured as volume fraction) fold changes of biofilms of matrix-protein deletion mutants in comparison to untreated biofilms. Data are mean ± s.e.m., $n=15$ (WT, −Tet), 9 (WT, +Tet), 10 (Δ*rbmC*, −Tet), 10 (Δ*rbmC*, +Tet), 15 (Δ*bap1*, −Tet), 8 (Δ*bap1*, +Tet) 18 (Δ*rbmA*, −Tet), 11 (Δ*rbmA*, +Tet); samples correspond to different biofilms. **c**, Cell volume and cell density fold-changes of RbmA mutants (D97A, D97K and R234A) with different conformations of RbmA structure. Data shown as mean ± s.e.m.; $n=15$ (WT, −Tet), 9 (WT, +Tet), 16 (D97A, −Tet), 19 (D97A, +Tet), 19 (D97K, −Tet), 10 (D97K, +Tet), 9 (R234A, -Tet), 10 (R234A, +Tet) 18 (Δ*rbmA*, −Tet) and 11 (Δ*rbmA*, +Tet); samples correspond to different biofilms. **d**, During antibiotic exposure, cells (labelled cyan using mTFP1) separate from the matrix (labelled yellow, using a fluorescent antibody against RbmA–His). The magnified inset shows individual cells detaching from RbmA during tetracycline treatment (indicated by red arrows, which show the same region of the biofilm in both panels). Images are representative of $n=5$ different biofilms. **e**, Heat maps show the average RbmA–His immunofluorescence surrounding each cell as a function of time and cellular distance from the biofilm boundary for tetracycline-treated (left) and untreated control (right) biofilms. Heat maps are representative of $n=5$ different biofilms. **f**, Cell density of Δ*rbmA* p*BAD::rbmA* biofilms as a function of arabinose concentration. Data are mean ± s.e.m., $n=7$ (0% arabinose), 12 (0.2%), 11 (0.3%), 16 (0.5%), 10 (1%), 18 (2%) and 14 (5%) samples; samples correspond to different biofilms. **g**, Fold change in cell density (comparing 6 h and 0 h of tetracycline treatment) of biofilms grown from the Δ*rbmA* p*BAD::rbmA* strain, as a function of arabinose concentration. Data are mean ± s.e.m., $n=5$ (0% arabinose), 12 (0.2%), 11 (0.3%), 16 (0.5%), 10 (1%), 18 (2%) and 14 (5%) samples; samples correspond to a different biofilms. **h**, Heat maps of simulated biofilms that were subject to a linear decrease in cell–cell attraction over 7 h (left), a linear increase in cell volume over 6 h (middle) or both effects together (right); $n=3$ simulation runs. **i**, Fold changes in cell volume and cell density of tetracycline-treated biofilms grown from strains that lack proteases involved in the processing of the matrix protein RbmA (Δ*hapA*, Δ*prtV* and Δ*ivaP*), or the enzyme RbmB (mean ± s.e.m., $n=17$ (WT), 8 (Δ*hapA*), 16 (Δ*prtV*), 3 (Δ*ivaP*) and 15 (Δ*rbmB*)). **j**, Fold changes in cell density of wild-type biofilms carrying the P*tac*::*rbmB* construct on a plasmid or an empty vector with IPTG induction (mean ± s.e.m., $n=16$ for P*tac*::*rbmB*, $n=11$ for control). In **i**,**j**, each sample corresponds to a different biofilm. Statistical significances were calculated using one-way ANOVA with Bonferroni's correction. Statistically non-significant differences (NS) in **i** correspond to $P=0.43$, 0.99, 0.59, 0.34, 0.99, 0.99 and 0.99 (left to right, respectively). $^{*}P<0.05$, $^{**}P<0.01$, $^{***}P<0.001$ and $^{****}P<0.0001$. Images in **a**,**d** were acquired 2 μm above the coverslip. WT, wild type.

VPS[28,36]. Should the RbmA-mediated bonds between cells be broken—for example, due to a reduced number of RbmA bonds per cell surface area following the cell volume increase—the balance between attraction and repulsion would be tipped and the cell density would decrease. To test this hypothesis, we used individual-based simulations that use an accurate and calibrated representation of mechanical cell–cell interactions in *V. cholerae* biofilms, enabling us to tune key parameters, including cell volume and cell–cell attraction and repulsion[28]. Using these simulations, we determined that a reduction in cell–cell attraction causes a decrease in cell density, but this alteration alone was not sufficient to recapitulate the pattern of biofilm volume expansion seen experimentally (Fig. 3h, left and Extended Data Fig. 8a,c). Similarly, increasing the cell volume without modifying the cell–cell attraction also fails to recapitulate the architectural changes seen in live biofilms (Fig. 3h, middle). However, when the cell–cell attraction is decreased and the cell volume is simultaneously increased, our simulations reproduce the architectural changes observed in experimental biofilms treated with antibiotics (Fig. 3h, right and Extended Data Fig. 8b,c). These results indicate that after the cells detach from the matrix, the observed changes in the biofilm architecture are primarily due to changes in the mechanical interactions between cells during tetracycline treatment and the accompanying increase in cell volume.

The profound changes in biofilm architecture that result from transient antibiotic exposure could potentially open up niches for external cells to colonize and invade the antibiotic-treated biofilms. Similarly, the dissociation of cells from their matrix during

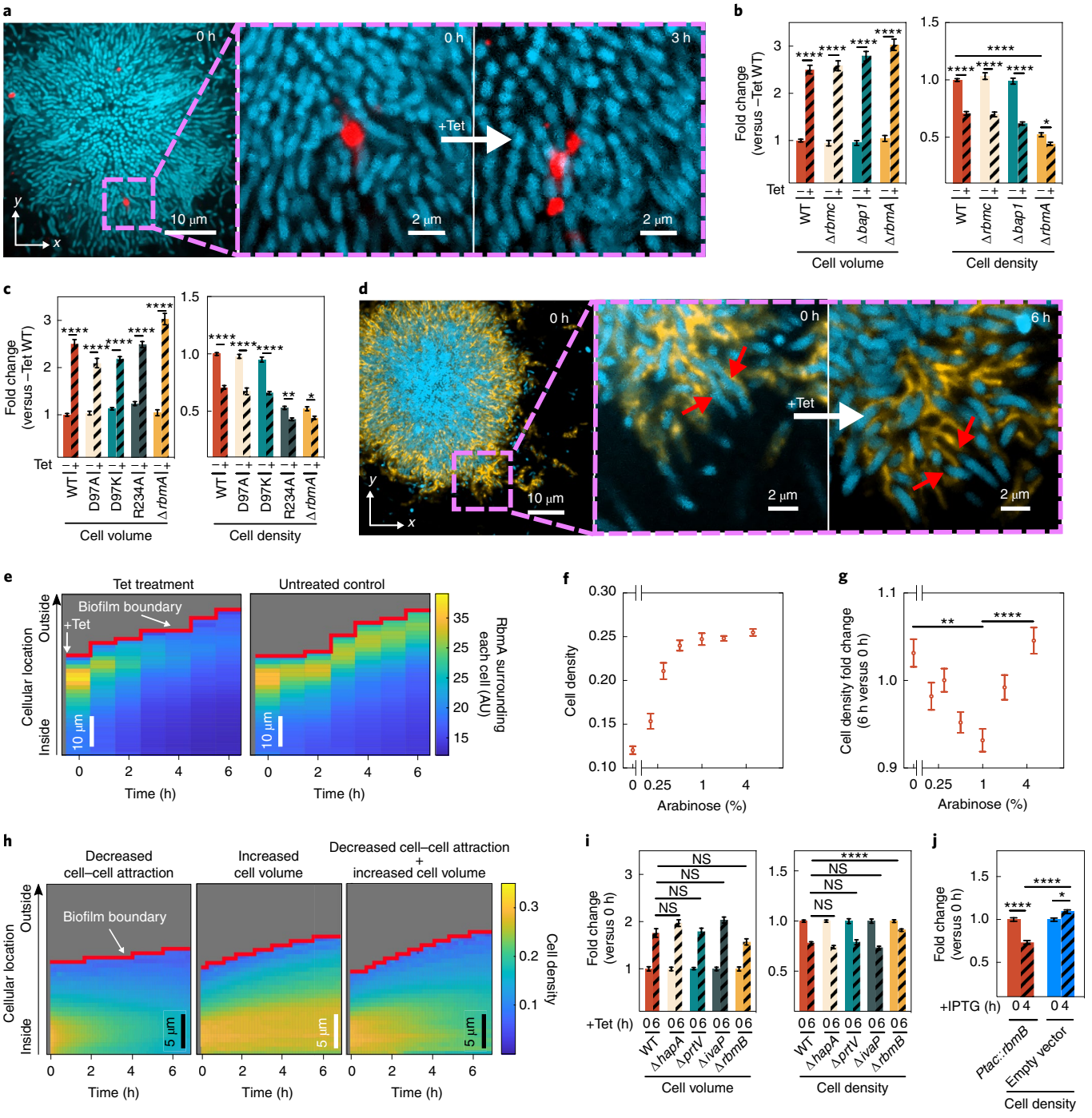

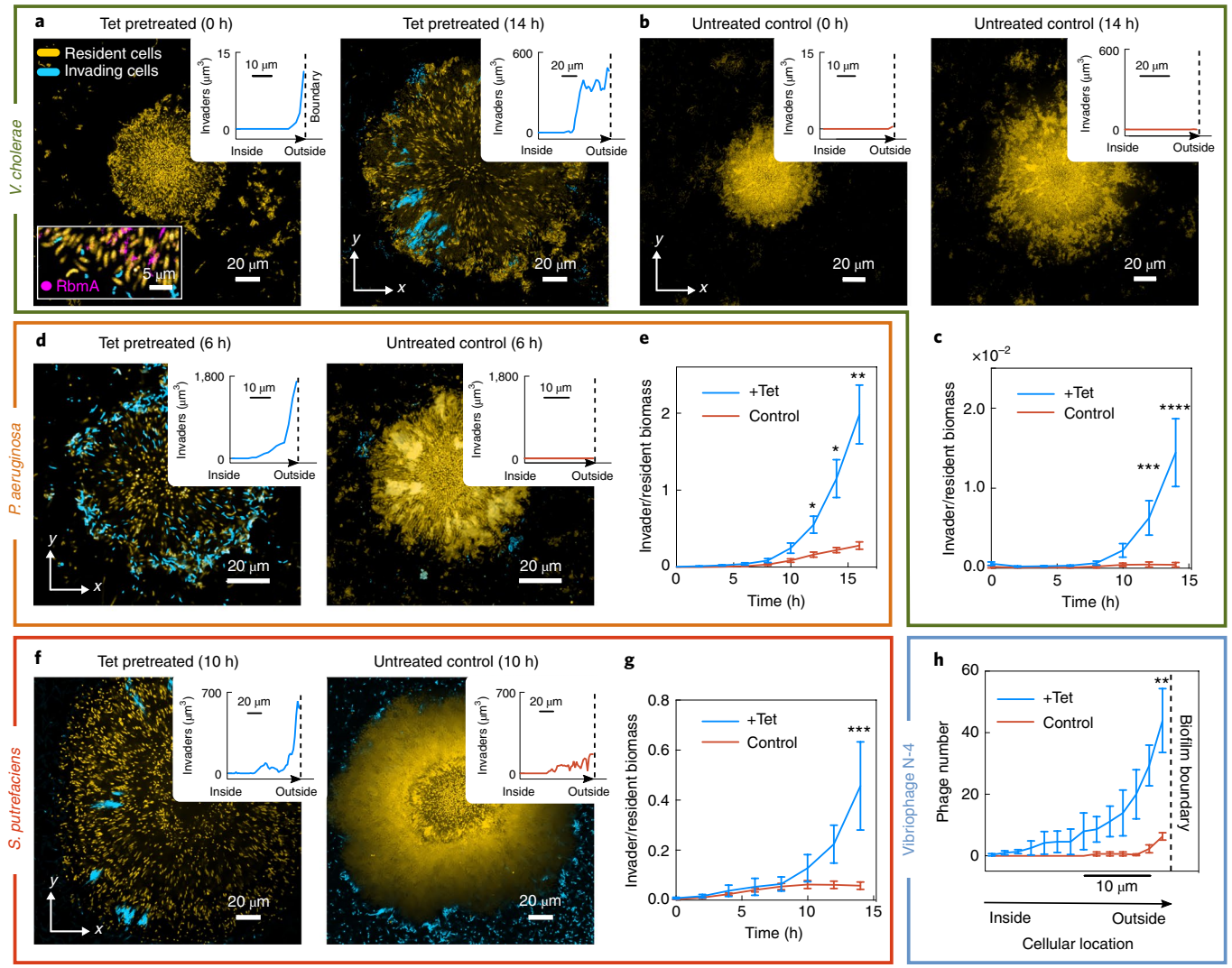

Fig. 4 | Antibiotic-treated biofilms are susceptible to colonization and invasion. a, Confocal *xy* slices of a resident *V. cholerae* wild-type biofilm, expressing mKOκ constitutively (cells shown in yellow). The resident biofilm underwent tetracycline treatment for 6 h, followed by 2 h exposure to invader cells (cyan), which are isogenic except for the fluorescent protein they express (sfGFP instead of mKOκ). Following exposure to planktonic invader cells, the medium was exchanged to fresh, sterile medium and the imaging was started (labelled 0 h here). The inset at 0 h shows a biofilm colonized by invader cells in which RbmA is visualized using immunofluorescence (magenta). Another inset shows the location where planktonic cells have colonized the resident biofilm, measured as a distance from the biofilm boundary. Replicate experiments are shown in Extended Data Fig. 9a,b. Cyan cells colonize the inside and periphery of biofilms, but rarely attach to the glass surface. **b**, Confocal *xy* slices of a control biofilm (not treated with tetracycline) exposed to *V. cholerae* invader cells for the same duration. Very few cells attach to the glass surface, and none to the resident biofilm, as described in Methods. Images in **a**,**b** are representative of eight different biofilms. **c**, Quantification of invader biomass divided by resident biomass during invasion of a *V. cholerae* biofilm population; data are mean ± s.e.m., $n = 8$ for +Tet and $n = 11$ for control conditions. **d**, Confocal *xy* slice of a tetracycline-treated or control resident *V. cholerae* biofilm invaded by *P. aeruginosa*, following the same protocol as in **a**. Images are representative of 12 different biofilms. **e**, *P. aeruginosa* invader biomass normalized by *V. cholerae* resident biomass; data are mean ± s.e.m., $n = 12$ for +Tet and $n = 11$ for control. **f**, Confocal *xy* slice of a tetracycline-treated or control resident *V. cholerae* biofilm invaded by *S. putrefaciens*, following the same protocol as in **a**. Images are representative of eight different biofilms. **g**, *S. putrefaciens* invader biomass normalized by *V. cholerae* resident biomass; mean ± s.e.m., $n = 12$ for +Tet and $n = 8$ for controls. **h**, Quantification of number of vibriophage N-4 virions as a function of position for tetracycline-treated biofilms and untreated control biofilms after 6 h of phage exposure; data are mean ± s.e.m., $n = 5$ for +Tet and $n = 3$ for controls. Images of phage invasion of biofilms are shown in Extended Data Fig. 9c. Images shown in **a**,**b**,**d**,**f** were acquired 2 μm above the substrate. Sample sizes (n) correspond to different biofilms. Statistical significances were calculated using two-way ANOVA with Bonferroni's correction. $^{*}P < 0.05$, $^{**}P < 0.01$, $^{***}P < 0.001$ and $^{****}P < 0.0001$.

antibiotic exposure may also enable phage entry into the biofilm, which is otherwise prevented by matrix[37].

To test these hypotheses, we first exposed tetracycline-treated *V. cholerae* biofilms to planktonic cultures of isogenic cells expressing a different fluorescent protein. Tetracycline-treated biofilms were indeed susceptible to colonization of their interior (Fig. 4a and Extended Data Fig. 9a,b); when the medium flowing through the growth channels was switched back to antibiotic-free medium, the resident biofilm strain and the colonizing strain proceeded to coexist in the biofilm, with the colonizer increasing in frequency to invade the biofilm population (Fig. 4c). In control experiments without antibiotic treatment, biofilms were highly resistant to

colonization and population invasion (Fig. 4b), consistent with previous investigations[38]. We also observed that bacterial species which share the natural marine and estuarine habitats with *V. cholerae*, such as *Shewanella putrefaciens*[39] and *Pseudomonas aeruginosa*[40], can also colonize and invade tetracycline-treated *V. cholerae* biofilm populations (Fig. 4d–g). Given this susceptibility to population invasion by other bacterial species, we tested whether bacteriophages, which are the primary predator of *V. cholerae* in environmental habitats, could also invade antibiotic-treated biofilms. By exposing *V. cholerae* biofilms to tetracycline and the vibriophage N-4 for 6 h, we observed an accumulation of phages in the outer region of the antibiotic-treated biofilms, in contrast to control biofilms (Fig. 4h and Extended Data Fig. 9c). In sum, these experiments demonstrate how architectural changes induced by antibiotic treatment can severely affect the ecological succession[41] of *V. cholerae* biofilm communities, and we speculate that architectural changes during antimicrobial treatment could have a key role in invasion susceptibility and succession of microbial communities in general.

The ubiquity of biofilm formation in microbial ecology is well-accepted, but we are still in the early stages of understanding how cell-level responses to the local environment translate to the emergent collective responses of biofilm communities. Here we have shown that even transient exposure to translation inhibitors causes changes in cell shape and physiology that yield large-scale alterations of biofilm architecture. The loosening of cell-matrix associations that occurs following antibiotic exposure, in turn, markedly alters community ecology by allowing new cells and phages to invade the community that would otherwise be unable to do so. The unicellular and multicellular processes identified here highlight mechanistic causes underlying ecological succession of microbial communities in response to antimicrobial therapeutics.

Methods

Media and strains. All *V. cholerae* strains used in this study are derivatives of the wild-type *V. cholerae* O1 biovar El Tor strain N16961. *V. cholerae* deletion mutations were created using plasmids derived from the pKAS32 suicide plasmid, harboured in *Escherichia coli* S17-1 λpir[27,42]. Plasmids for chromosomal deletions were made by amplification of the 1 kb flanking regions of the corresponding gene. The PCR product was cloned into the suicide plasmid and transformed into *E. coli*. Plasmids were transferred into *V. cholerae* by conjugation. Fluorescent protein expression constructs were introduced into the *lacZ* locus and screening was carried out using a β-galactosidase colony colour conversion assay. For *rbmB* overexpression experiments (Fig. 3j), *V. cholerae* strains carrying plasmids were grown with gentamicin (30 μg ml^{-1}) throughout all experiments.

All experiments with biofilms or single cells were performed in M9 minimal medium (M9 minimal salts; M6030, Sigma), supplemented with 2 mM $MgSO_4$, 100 mM $CaCl_2$, MEM vitamins, 0.5% glucose and 15 mM triethanolamine (pH 7.1), referred to in the manuscript as 'M9 medium' for simplicity, unless stated otherwise. For *S. putrefaciens* invasion assays, biofilms were grown in tryptone broth (10 g l^{-1} tryptone) instead of M9 medium. Overnight cultures were grown in shaking (250 r.p.m.) liquid Luria–Bertani–Miller broth (LB-Miller; 10 g l^{-1} tryptone, 5 g l^{-1} yeast extract and 10 g l^{-1} NaCl) at 37 °C. Detailed lists of all strains, plasmids and DNA oligonucleotides used in this study are provided in Supplementary Tables 1–3, respectively.

MIC determination. For MIC determination, the wild-type *V. cholerae* N16961 strain (KDV101) was grown in LB-Miller overnight at 37 °C with shaking at 250 r.p.m. The overnight cultures were then diluted 1:50 in M9 medium (see description of medium above) and grown at 28 °C until exponential phase (absorbance at 600 nm (OD_{600}) of 0.5–0.6). The OD_{600} was then adjusted to 0.5 and the suspension was used to inoculate a 96-well plate (82.1581.001, Sarstedt) containing different antibiotic concentrations. The liquid volume per well was 180 μl and the initial inoculation OD_{600} in each well was 0.05. The 96-well plate was then incubated at 28 °C with shaking in a microtitre plate reader (Spark 10 M, Tecan) for 20 h. MICs were calculated from two independent experiments with two technical replicates per experiment (Extended Data Fig. 1c,d and Supplementary Table 4).

Flow chamber biofilm experiments. *V. cholerae* biofilms were grown in microfluidic flow chambers made from polydimethylsiloxane bonded to glass coverslips using an oxygen plasma, with four to eight channels on a single coverslip, as previously described[26]. The microfluidic channels measured 500 μm in width, 100 μm in height and 7 mm in length. Channels were inoculated with overnight cultures of *V. cholerae* strains. Following inoculation, the cells were given 1 h at room temperature (24–26 °C) to attach to the surface of the channel before fresh M9 medium was flowed through the channel at a flow rate of 50 μl min^{-1} for 45 s, to wash away non-attached cells and to completely replace the LB-Miller medium from the channel. The flow rate of fresh M9 medium was then set to 0.05 μl min^{-1} for the remainder of the experiment, corresponding to an average flow speed of 17 μm s^{-1} in the channel. Flow rates were maintained using a syringe pump (picoPlus, Harvard Apparatus). The flow chamber, M9 medium and syringe pump were maintained at room temperature (24–26 °C) for the duration of all experiments.

Exposure of biofilms to antibiotics. To test the influence of different antibiotics on mature biofilms, biofilms were grown for 24 h in M9 medium before being exposed to one of the following antibiotics: rifampicin (6 μg ml^{-1}), ciprofloxacin (0.5 μg ml^{-1}), erythromycin (200 μg ml^{-1}), kanamycin (200 μg ml^{-1}), ampicillin (400 μg ml^{-1}), tetracycline (3 μg ml^{-1}), chloramphenicol (10 μg ml^{-1}), trimethoprim (10 μg ml^{-1}) or ceftibuten (50 μg ml^{-1}). The concentrations for each antibiotic were at least two times the MIC, which was determined for our strain and media conditions using a microtiter plate reader (Spark 10 M, Tecan), as described in the section on MIC measurements above. For ampicillin and ceftibuten, it was not possible to determine a MIC. Instead, we used concentrations that cause changes in cell morphology due to cell-wall loss. After exposure to an antibiotic for 24 h, the biofilms were stained with 4 μM SYTO 9 (S34854, ThermoFisher).

To test for cell death during antibiotic exposure, propidium iodide (7.5 μM) was used as a reporter—cells that have a compromised cell envelope are stained red by propidium iodide. During time-series imaging of cell death inside biofilms, a strain carrying a P*tac* promoter fusion to *mTFP1* (KDV392) was used (Extended Data Fig. 4).

To investigate biofilm architectural modifications in response to antibiotic treatment in detail, tetracycline was chosen as the main antibiotic for this study, as it is a commonly used treatment against cholera infections[25]. To avoid investigations of architectural modifications due to cell death, exposure to tetracycline was limited to 6 h in all experiments described in this manuscript, except for those investigating cell death in biofilms as a function of treatment time (Extended Data Fig. 4). For the experiments involving a constitutively expressed fluorescent protein for biofilm architecture quantification, we used strains carrying a P*tac* promoter fused to the genes coding for the fluorescent reporters mKusabira orange kappa (mKOκ), a red fluorescent protein (mRuby3), superfolder green fluorescent protein (sfGFP) or bright teal fluorescent protein (mTFP1) at the *lacZ* locus.

Exposure of individual adherent cells to antibiotics. An overnight culture of a wild-type strain carrying the constitutively expressed P*tac*::*mKOκ* system on the chromosome (strain KDV103) was back-diluted 1:100 in M9 medium and grown under shaking conditions at 250 r.p.m. until OD_{600} = 0.45–0.55. This suspension was then used to inoculate a diffuse monolayer of cells on the glass substratum of microfluidic devices, which were kept at room temperature (24–26 °C). After 30 min, flow was initiated at 0.05 μl min^{-1} using M9 with or without tetracycline. The flow chambers were kept at room temperature throughout the experiment.

Antibiotics treatments in liquid culture and metabolomics. Overnight cultures were back-diluted 1:100 in M9 medium and grown at 25 °C in shaking conditions at 250 r.p.m. until the culture reached OD_{600} = 0.45–0.55. At this point, tetracycline or an equivalent volume of methanol (the stock solvent for tetracycline, as a negative control) was added to the cultures. To measure the cell size as a function of time after tetracycline or clean methanol was added, aliquots of the culture were taken every hour and imaged by microscopy. For metabolome analysis, samples were collected after 2 h for both treatments (tetracycline- and non-tetracycline-exposed cultures).

Metabolome analyses were performed as previously described[43], with minor modifications. In brief, for sampling of metabolites by filtration, 1 ml of culture with an OD_{600} of 0.5 was vacuum-filtered on a 0.45 μm pore-size membrane (HVLP02500, Merck Millipore) to remove the spent medium, before cells were exposed to M9 medium containing U-13C glucose (99%, Cambridge Isotope Laboratories) for 0, 30, 90, 120 or 150 s. Afterwards, filters were immediately transferred to a mixture of acetonitrile:methanol:water (40:40:20) and stored at −20 °C. Metabolite extracts were centrifuged for 15 min at 13,000 r.p.m. at −9 °C to remove cellular debris. The supernatant was used directly for liquid chromatography with tandem mass spectrometry.

RbmA complementation, titration and immunolabelling. To control the amount of RbmA produced by cells, we constructed a Δ*rbmA* clean deletion strain into which *rbmA*-His_6 was re-introduced under the control of the tightly regulated, arabinose-inducible p*BAD* promoter. This construct was inserted by allelic exchange into the *V. cholerae* chromosome at the *lacZ* locus (strain KDV859). The following arabinose concentrations were used to induce RbmA expression in biofilms: 0.2, 0.3, 0.5, 1, 2 and 5%.

To stain extracellular RmbA, a strain carrying the P*tac* promoter fused to *mTFP1* and *rbmA*-His_6 (KDV605) was used. After 4 h of biofilm growth, a

His-tag monoclonal antibody conjugated to Alexa Fluor 555 was added at a final concentration of 1 μg ml^{-1} (ThermoFisher, MA1-135-A555) to the inflowing M9 medium. To avoid nonspecific binding, bovine serum albumin (1 mg ml^{-1}) was added to the medium together with the antibody, as described previously[31].

Matrix movement assay using fluorescent beads. Biofilms of the sfGFP-expressing wild-type strain KDV311 were grown for 24 h in presence of red fluorescent beads of diameter 0.1 μm (F8887, ThermoFisher) in the medium. This led to an incorporation of beads into the extracellular matrix of the biofilms. Subsequently, the medium was exchanged for fresh M9 medium without beads and tetracycline was added. From this point, the biofilms were imaged for 6 h with a time resolution of 1 h.

RbmB controlled overexpression. Biofilms of the mKOκ-expressing wild-type strain carrying either a plasmid-based isopropylthiogalactoside (IPTG)-inducible *rbmB* expression construct (KDV1070) or an empty vector (KDV1078) were grown for 24 h before addition of 1 μM IPTG. Starting from this time point, biofilms were imaged for 4 h with a time resolution of 1 h.

Bacterial biofilm-invasion assay. Biofilms of the mKOκ-expressing wild-type strain KDV103 were grown for 24 h before the inflowing M9 medium was exchanged to one containing tetracycline for 6 h. As a control treatment, M9 medium without tetracycline was added for 6 h. Separately, at the same time, an overnight culture of the sfGFP-expressing wild-type strain KDV311 or an overnight culture of KDP54, a *P. aeruginosa* PAO1 strain expressing sfGFP was diluted 1:200 in M9 and grown at 37 °C under shaking conditions (250 r.p.m.) until exponential phase (OD_{600} = 0.4). After the biofilms were exposed to either tetracycline or control treatment for 6 h, the exponential phase culture of KDV311 or KDP54 was introduced into the flow channel containing the resident KDV103 biofilms at a flow rate of 0.05 μl min^{-1}. After the sfGFP-expressing planktonic cells were allowed to colonize and invade the resident biofilms for 2 h, the inflowing medium was exchanged to sterile M9 medium without any cells. Starting from this time point (labelled as '0 h' in Fig. 4 and Extended Data Fig. 9a,b), biofilms were imaged for 24 h with a time resolution of 2 h.

During experiments in which *V. cholerae* resident biofilms were exposed to planktonic *V. cholerae* cells (Fig. 4a,b and Extended Data Fig. 9a,b), the planktonic cells rarely attached to the glass surface in either conditions (tetracycline-pretreated or untreated control) during the 2 h initial time window of exposure to the resident biofilms. There was significantly more attachment and colonization to tetracycline-treated biofilms compared with untreated control biofilms at 0 h (Fig. 4a,b), and therefore much more biomass accumulation of the invader cells in the tetracycline-treated condition compared with the control. Some of the accumulated invader biomass in the tetracycline-treated condition dispersed and colonized the glass surface surrounding the biofilm, whereas in the control condition there was not enough invader biomass to substantially colonize the glass surface.

For *S. putrefaciens* (CN-32 wild-type strain, KDM77) invasion experiments, the same protocol was used as described above for the *V. cholerae* and *P. aeruginosa* invasion experiments, except for the following modifications. All *V. cholerae* resident biofilms were grown in tryptone broth. To obtain an exponentially growing culture of *S. putrefaciens*, the frozen stock was streaked on a LB-Miller agar plate, which was incubated at room temperature. From this plate, colonies were picked to inoculate a LB-Miller liquid culture, which was grown under shaking conditions at 28 °C. Using this culture, another flask containing tryptone broth was inoculated with a 1:200 dilution and grown at 28 °C until exponential phase (OD_{600} = 0.4). This culture was used as the culture of planktonic invader cells for the invasion assay.

Biofilm phage invasion assay and vibriophage N-4 fluorescent labelling. Bacteriophage were labelled as described previously[37]. In brief, 100 μl of purified vibriophage with a concentration of 1×10^{12} plaque-forming units (PFU) per ml were mixed with sodium carbonate (0.1 M final concentration) and then incubated with 0.1 mg Alexa Fluor 488 5-TFP (A30005, ThermoFisher Scientific) for 1 h at room temperature under continuous shaking. The reaction mixture was first dialysed at 4 °C against 500 ml PBS for 3 h and then dialysed overnight at 4 °C against 2 l of PBS. This was done to separate phage from unbound dye. This stock of fluorescently labelled phage was stored at 4 °C.

Biofilms of the mRuby3-expressing *V. cholerae* wild-type strain (KDV657) were grown for 24 h, before the inflowing M9 medium was exchanged to contain tetracycline for 6 h and fluorescently labelled phage (a 1:100 dilution of the fluorescently labelled phage stock). As a control treatment, M9 medium without tetracycline, but containing the same concentration of vibriophage was added for 6 h. Biofilms were imaged for the 6 h of phage exposure with a time resolution of 2 h (Extended Data Fig. 9c).

Microscopy and image analysis. Biofilm architecture was imaged and analysed in the biofilm volume between z = 0 μm and z = 10 μm (that is, the part of the biofilm within the 10 μm of the glass substrate) for most experiments, unless indicated otherwise in the figure caption. In control experiments, we determined that this lower part of the biofilm had an identical biofilm architecture to the complete biofilm in terms of cell volume, cell aspect ratio and cell density, both in terms of mean values (Extended Data Fig. 10a) and in terms of spatially resolved values at different time points (Extended Data Fig. 10b,c). Because of photobleaching and phototoxicity it was not possible to acquire image time series during antibiotic treatment of the whole biofilm at single-cell resolution, so for most experiments only the representative lowest 10 μm of the biofilm were imaged. All imaging was performed using a Yokogawa spinning-disc confocal unit, mounted on a Nikon Ti-E inverted microscope using a ×100 silicone oil objective (numerical aperture (NA) 1.35, Olympus). For confocal imaging, pictures were taken with a z-step size of 0.4 μm.

For biofilm-invasion assays, we used a Nikon ×60 NA 1.4 oil objective on the spinning-disc confocal microscope. For invasion experiments that required three-colour imaging (Fig. 4a), we used a point-scanning confocal microscope (LSM 880, Zeiss), equipped with a tuneable emission spectrum selector for each fluorescence channel, and a Zeiss ×60 NA 1.4 oil objective.

Image analysis of biofilms was performed using Matlab (Mathworks), as described previously[27,28]. After segmentation of all cells in the biofilm images, we calculated for each cell the aspect ratio, the matrix density surrounding each cell (for experiments in which RbmA was labelled fluorescently), the cell density at each cellular location and each cell's distance to the biofilm boundary. The biofilm boundary is defined as the interface between the biofilm and the liquid growth medium. Each of these quantifications is explained in detail below.

To calculate the cellular aspect ratio, an ellipsoid was fitted into each cell and the longest axis of the ellipsoid was used as cell length and the shortest as cell width. The cell aspect ratio is the ratio of cell length and cell width.

To calculate the location of each cell relative to the biofilm boundary, which is the spatial metric used to quantify the cellular location in the biofilms throughout the manuscript, we calculated the shortest distance from each cell to the interface between the biofilm and the liquid growth medium. Qualitatively, this spatial metric for the cellular location in the biofilm corresponds to the shortest distance that nutrients from the growth medium would have to diffuse to reach the cell. We note that *V. cholerae* biofilm communities grow into colonies with roughly hemispherical shape in our conditions[27,28]. If the colony morphology would be an exact hemisphere, then the distance of each cell to the biofilm boundary would correspond to a path along the radial direction in spherical coordinates, where the origin would be at the centre of mass of the colony projected onto the z = 0 μm plane. Given that *V. cholerae* biofilms differ from exact hemispherical shapes, we opted to use the distance to the biofilm boundary as the spatial metric to quantify cellular location.

To compute the kymograph heat maps for a given parameter (such as the cell volume or cell aspect ratio) at each time point, the parameter value of all cells with the same distance to the biofilm boundary was averaged, resulting in a value that corresponds to the value of a particular pixel in the heat map. This calculation was then performed for all distances to the biofilm boundary and all time points to result in the heat map. We previously used such spatiotemporal heat maps of biofilms to quantify spatiotemporal biofilm development[28] and biofilm dispersal[27].

To calculate the cell density of biofilms, we used a measurement of volume fraction. We created a sphere of 3 μm radius starting from the centroid of each cell. Then, we calculated how much of the volume of the sphere, excluding the volume of the cell used to create the sphere, was occupied by other cells.

To quantify the RbmA-matrix density surrounding each cell, we measured the fluorescent signal of immunofluorescently labelled RbmA–His_6 that surrounds each cell within a 0.2 μm-thick 3D shell around each cell. The strain with the His-tagged RbmA used for immunostaining phenocopies the wild-type strain before and during antibiotic treatment (Extended Data Fig. 6).

To quantify the biofilm-invasion phenotype (Fig. 4) we measured the total biomass of the invader cells between z = 0 μm and z = 10 μm (that is, the lowest 10 μm of the biofilm) and divided this value by the total biomass of cells within the lowest 10 μm of the resident biofilm.

To analyse images of planktonic cells or single cells that are adherent to a surface (Fig. 2a), MicrobeJ was used[44].

Crystal violet assay. Crystal violet experiments were performed as described previously[45], with some modifications. In brief, strain KDV103 and strain KDV115 were grown overnight in LB-Miller at 37 °C, shaking at 250 r.p.m. These cultures were then diluted 1:1,000 in M9 and the resulting suspension was used to inoculate a 96-well plate, which was then incubated for biofilm growth at room temperature. At different time points, the biomass was measured using crystal violet methods as described previously[45].

For testing antibiotic exposure of biofilms with the crystal violet assay, biofilms were grown for 14 h in a 96-well plate (82.1581.001, Sarstedt). At this time, tetracycline, trimethoprim, chloramphenicol, kanamycin or erythromycin were added, reaching a final concentration of 3 μg ml^{-1}, 10 μg ml^{-1}, 10 μg ml^{-1}, 200 μg ml^{-1} or 200 μg ml^{-1}, respectively. As a control, the same volume of M9 medium without tetracycline was added to a different well. The treated and untreated wells were then incubated for 6 h. After this incubation period, the biomass was measured using crystal violet. All measurements were performed using a microplate reader (Tecan Spark 10 M). For each measurement, the data were averaged from eight wells (technical replicates) per experiment, and n = 3 independent biological replicates.

Biofilm simulations. Biofilm formation was simulated using the agent-based framework described by Hartmann et al.[28]. Cells are modelled as ellipsoids interacting with the channel wall via a repulsive boundary potential, and with other cells via an interaction potential. This interaction potential accounts for effective cell–cell repulsion due to steric forces and VPS production, and for cell–cell attraction mediated by adhesion molecules such as RbmA[32]. For two cells γ and β, we let l_γ and l_β be their lengths and d_γ and d_β their widths in μm; $\hat{\mathbf{n}}_\lambda$ and $\hat{\mathbf{n}}_\beta$ are their orientation vectors, $r_{\gamma\beta}$ is the distance between their centroids, and $\hat{\mathbf{r}}_{\gamma\beta}$ is the unit vector pointing from the centroid of cell γ to the centroid of cell β. The pairwise interaction potential $U_{\gamma\beta}$ between cell γ and cell β is

$$U_{\gamma\beta} = \epsilon_0\epsilon_1\left(\exp\left(-\rho_{\gamma\beta}^2/\lambda_r^2\right) + \frac{\nu}{1+\exp\left(\left(\rho_a-\rho_{\gamma\beta}\right)/\lambda_a\right)}\right) \quad (1)$$

where $\rho_{\gamma\beta}=r_{\gamma\beta}/\sigma$ is the shape-normalized cell–cell distance between two cells in μm (ref. [28]). The dimensionless range parameter $\sigma(l_\gamma, l_\beta, d_\gamma, d_\beta, \hat{\mathbf{n}}_\gamma, \hat{\mathbf{n}}_\beta, \hat{\mathbf{r}}_{\gamma\beta})$ depends on the cells' ellipsoidal shapes, relative positions and the relative orientations. The overall strength of $U_{\gamma\beta}$ is set by the energy scale ϵ_0, scaled by the dimensionless geometric factor $\epsilon_1(l_\gamma, l_\beta, d_\gamma, d_\beta, \hat{\mathbf{n}}_\gamma, \hat{\mathbf{n}}_\beta)$ that accounts for the shapes and the relative orientations of the cells[28]. The range of cell–cell repulsion is set by length parameter λ_r. The relative strength of the cell–cell attraction is set by dimensionless parameter ν. The length parameter ρ_a determines the energetically preferred cell–cell distance, and λ_a is the gradient of the attractive barrier. The model parameters ϵ_0, λ_r, ν, ρ_a and λ_a were obtained by fitting simulated biofilms to experimental biofilms, using the mean square distance of a feature vector as a metric, which incorporated 14 different architectural parameters and their temporal development[28]. For $\epsilon_0=5\times10^{-20}$ J, $\lambda_r=1.16$ μm, $\nu=0.13$, $\lambda_a=0.11$ μm and $\rho_a=2.0$ μm, the simulations yield biofilms with quantitatively and qualitatively similar architectural dynamics as those observed in the experiments for biofilm sizes up to approximately 2,000 cells (for other simulation parameters and detailed comparisons between simulations and experimental biofilms, see Hartmann et al.[28]).

Using this model, biofilm growth was simulated until the biofilm size reached 1,000 cells. Then, tetracycline-treatment was simulated by stopping cell division and probing three different effects: (1) the cell–cell attraction was linearly decreased to zero over time with varying total duration (0–10 h), following the quantitative relationship between varying RbmA levels and the model parameters ϵ_0, λ_r, ν, ρ_a and λ_a that was established by Hartmann et al.[28], (2) the volume of each cell was increased according to the single cell volume growth rate observed in biofilms after tetracycline-treatment, and (3) the joint effects of loss of cell–cell attraction and increase in cell volume were applied together. In all cases, the cell density of the simulated biofilm was monitored as a function of tetracycline-treatment time and as a function of the shortest distance to the boundary between the biofilm and the growth medium, using the same analysis scripts as for the experimental biofilms.

Statistical analysis. All statistical tests indicated in figure legends were performed using GraphPad Prism v.8.1.1.

Reporting Summary. Further information on research design is available in the Nature Research Reporting Summary linked to this article.

Data availability

Raw and analysed data that support the findings of this study are available from the corresponding author upon request.

Code availability

Our open-source and user-friendly biofilm image analysis software tool BiofilmQ[46] is available online (https://drescherlab.org/data/biofilmQ/). The raw developer-level code used to analyse data is available from the corresponding author upon request.

Received: 5 December 2018; Accepted: 6 September 2019;
Published online: 28 October 2019

References

1. D'Costa, V. M. et al. Antibiotic resistance is ancient. *Nature* **477**, 457–461 (2011).
2. Baym, M. et al. Spatiotemporal microbial evolution on antibiotic landscapes. *Science* **353**, 1147–1151 (2016).
3. Hoffman, L. R. et al. Aminoglycoside antibiotics induce bacterial biofilm formation. *Nature* **436**, 1171–1175 (2005).
4. Koch, G. et al. Evolution of resistance to a last-resort antibiotic in *Staphylococcus aureus* via bacterial competition. *Cell* **158**, 1060–1071 (2014).
5. Jenssen, H., Hamill, P. & Hancock, R. E. W. Peptide antimicrobial agents. *Clin. Microbiol. Rev.* **19**, 491–511 (2006).
6. Houry, A. et al. Bacterial swimmers that infiltrate and take over the biofilm matrix. *Proc. Natl Acad. Sci. USA* **109**, 13088–13093 (2012).
7. Andersson, D. I. & Hughes, D. Microbiological effects of sublethal levels of antibiotics. *Nat. Rev. Microbiol.* **12**, 465–478 (2014).
8. O'Neill, J. ed. *Antimicrobial Resistance: Tackling a Crisis for the Health and Wealth of Nations* (HM Government, 2014).
9. Van Acker, H., Van Dijck, P. & Coenye, T. Molecular mechanisms of antimicrobial tolerance and resistance in bacterial and fungal biofilms. *Trends Microbiol.* **22**, 326–333 (2014).
10. Lebeaux, D., Ghigo, J.-M. & Beloin, C. Biofilm-related infections: bridging the gap between clinical management and fundamental aspects of recalcitrance toward antibiotics. *Microbiol. Mol. Biol. Rev.* **78**, 510–543 (2014).
11. Koo, H., Allan, R. N., Howlin, R. P., Stoodley, P. & Hall-Stoodley, L. Targeting microbial biofilms: current and prospective therapeutic strategies. *Nat. Rev. Microbiol.* **15**, 740–755 (2017).
12. Meylan, S., Andrews, I. W. & Collins, J. J. Targeting antibiotic tolerance, pathogen by pathogen. *Cell* **172**, 1228–1238 (2018).
13. Garcia, L. G. et al. Antibiotic activity against small-colony variants of *Staphylococcus aureus*: review of in vitro, animal and clinical data. *J. Antimicrob. Chemother.* **68**, 1455–1464 (2013).
14. Kwan, B. W., Valenta, J. A., Benedik, M. J. & Wood, T. K. Arrested protein synthesis increases persister-like cell formation. *Antimicrob. Agents Chemother.* **57**, 1468–1473 (2013).
15. Grant, S. S. & Hung, D. T. Persistent bacterial infections, antibiotic tolerance, and the oxidative stress response. *Virulence* **4**, 273–283 (2013).
16. Brooun, A., Liu, S. & Lewis, K. A Dose-response study of antibiotic resistance in *Pseudomonas aeruginosa* biofilms. *Antimicrob. Agents Chemother.* **44**, 640–646 (2000).
17. Chua, S. L. et al. Selective labelling and eradication of antibiotic-tolerant bacterial populations in *Pseudomonas aeruginosa* biofilms. *Nat. Commun.* **7**, 10750 (2016).
18. Gupta, K., Marques, C. N. H., Petrova, O. E. & Sauer, K. Antimicrobial tolerance of *Pseudomonas aeruginosa* biofilms is activated during an early developmental stage and requires the two-component hybrid SagS. *J. Bacteriol.* **195**, 4975–4987 (2013).
19. Okshevsky, M. & Meyer, R. L. The role of extracellular DNA in the establishment, maintenance and perpetuation of bacterial biofilms. *Crit. Rev. Microbiol.* **41**, 341–352 (2015).
20. Mah, T.-F. et al. A genetic basis for *Pseudomonas aeruginosa* biofilm antibiotic resistance. *Nature* **426**, 306–310 (2003).
21. Nguyen, D. et al. Active starvation responses mediate antibiotic tolerance in biofilms and nutrient-limited bacteria. *Science* **334**, 982–986 (2011).
22. Høiby, N., Bjarnsholt, T., Givskov, M., Molin, S. & Ciofu, O. Antibiotic resistance of bacterial biofilms. *Int. J. Antimicrob. Agents* **35**, 322–332 (2010).
23. Tseng, B. S. et al. The extracellular matrix protects *Pseudomonas aeruginosa* biofilms by limiting the penetration of tobramycin. *Environ. Microbiol.* **15**, 2865–2878 (2013).
24. Dale, J. L., Nilson, J. L., Barnes, A. M. T. & Dunny, G. M. Restructuring of *Enterococcus faecalis* biofilm architecture in response to antibiotic-induced stress. *NPJ Biofilms Microbiomes* **3**, 15 (2017).
25. Wong, K. C., Brown, A. M., Luscombe, G. M., Wong, S. J. & Mendis, K. Antibiotic use for *Vibrio* infections: important insights from surveillance data. *BMC Infect. Dis.* **15**, 226 (2015).
26. Drescher, K. et al. Architectural transitions in *Vibrio cholerae* biofilms at single-cell resolution. *Proc. Natl Acad. Sci. USA* **113**, E2066–E2072 (2016).
27. Singh, P. K. et al. *Vibrio cholerae* combines individual and collective sensing to trigger biofilm dispersal. *Curr. Biol.* **27**, 3359–3366 (2017).
28. Hartmann, R. et al. Emergence of three-dimensional order and structure in growing biofilms. *Nat. Phys.* **15**, 251–256 (2019).
29. Adams, D. W. & Errington, J. Bacterial cell division: assembly, maintenance and disassembly of the Z ring. *Nat. Rev. Microbiol.* **7**, 642–653 (2009).
30. Stewart, E. J., Satorius, A. E., Younger, J. G. & Solomon, M. J. Role of environmental and antibiotic stress on *Staphylococcus epidermidis* biofilm microstructure. *Langmuir* **29**, 7017–7024 (2013).
31. Berk, V. et al. Molecular architecture and assembly principles of *Vibrio cholerae* biofilms. *Science* **337**, 236–239 (2012).
32. Fong, J. C. et al. Structural dynamics of RbmA governs plasticity of *Vibrio cholerae* biofilms. *eLife* **6**, 1–22 (2017).
33. Smith, D. R. et al. In situ proteolysis of the *Vibrio cholerae* matrix protein rbma promotes biofilm recruitment. *Proc. Natl Acad. Sci. USA* **112**, 10491–10496 (2015).
34. Fong, J. C. N. & Yildiz, F. H. The *rbmBCDEF* gene cluster modulates development of rugose colony morphology and biofilm formation in *Vibrio cholerae*. *J. Bacteriol.* **189**, 2319–2330 (2007).
35. Douarche, C., Allain, J.-M. & Raspaud, E. *Bacillus subtilis* bacteria generate an internal mechanical force within a biofilm. *Biophys. J.* **109**, 2195–2202 (2015).
36. Yan, J., Nadell, C. D., Stone, H. A., Wingreen, N. S. & Bassler, B. L. Extracellular-matrix-mediated osmotic pressure drives *Vibrio cholerae* biofilm expansion and cheater exclusion. *Nat. Commun.* **8**, 327 (2017).

37. Vidakovic, L., Singh, P. K., Hartmann, R., Nadell, C. D. & Drescher, K. Dynamic biofilm architecture confers individual and collective mechanisms of viral protection. *Nat. Microbiol.* **3**, 26–31 (2018).
38. Nadell, C. D., Drescher, K., Wingreen, N. S. & Bassler, B. L. Extracellular matrix structure governs invasion resistance in bacterial biofilms. *ISME J.* **9**, 1700–1709 (2015).
39. Jørgensen, B. R. & Huss, H. H. Growth and activity of *Shewanella putrefaciens* isolated from spoiling fish. *Int. J. Food Microbiol.* **9**, 51–62 (1989).
40. Kimata, N., Nishino, T., Suzuki, S. & Kogure, K. *Pseudomonas aeruginosa* isolated from marine environments in Tokyo bay. *Microb. Ecol.* **47**, 41–47 (2004).
41. Brislawn, C. J. et al. Forfeiting the priority effect: turnover defines biofilm community succession. *ISME J.* **13**, 1865–1877 (2019).
42. Skorupski, K. & Taylor, R. K. Positive selection vectors for allelic exchange. *Gene* **169**, 47–52 (1996).
43. Guder, J. C., Schramm, T., Sander, T. & Link, H. Time-optimized isotope ratio LC–MS/MS for high-throughput quantification of primary metabolites. *Anal. Chem.* **89**, 1624–1631 (2017).
44. Ducret, A., Quardokus, E. M. & Brun, Y. V. MicrobeJ, a tool for high throughput bacterial cell detection and quantitative analysis. *Nat. Microbiol.* **1**, 16077 (2016).
45. O'Toole, G. A. Microtiter dish biofilm formation assay. *J. Vis. Exp.* **47**, e2437 (2011).
46. Hartmann, R. et al. BiofilmQ, a software tool for quantitative image analysis of microbial biofilm communities. Preprint at *bioRxiv* https://doi.org/10.1101/735423 (2019).
47. Beyhan, S. & Yildiz, F. H. Smooth to rugose phase variation in *Vibrio cholerae* can be mediated by a single nucleotide change that targets c-di-GMP signalling pathway. *Mol. Microbiol* **63**, 995–1007 (2007).

Acknowledgements

We thank P. K. Singh, P. Pearce, S. Vaidya, M. Bayer, K. Neuhaus, E. Jimenez and K. Strenger for strains and support during this project, and thankfully acknowledge grants from the Max Planck Society, Human Frontier Science Program (CDA00084/2015-C), Deutsche Forschungsgemeinschaft (SFB 987), Behrens-Weise-Stiftung, Minna-James-Heineman-Stiftung and European Research Council (StG-716734) to K.D., the MIT-Germany MISTI Seed Fund Program to K.D. and J.D., and the James S. McDonnell Foundation (J.D.). C.D.N. is supported by the Alexander von Humboldt Foundation, National Science Foundation (MCB 1817342), a Burke Award from Dartmouth College, a pilot award from the Cystic Fibrosis Foundation (STANTO15RO) and NIH grant P20-GM113132 to the Dartmouth BioMT COBRE.

Author contributions

K.D. conceived, supervised and coordinated the project. C.D.N. and K.D. designed experiments. J.D. designed simulations. F.D.-P. and L.V. performed all biofilm experiments. F.D.-P. and L.V. performed liquid culture experiments. F.D.-P., M.L. and H.L. performed metabolite measurements and analysis. R.H. and H.J. developed image and data analysis methods. F.D.-P., R.H. and H.J. performed image analysis. R.H. and B.S. performed simulations. F.D.-P. and L.V. generated strains. F.H.Y. and K.M.T. developed strains and analysis ideas. All authors made important conceptual contributions to the project and interpreted results, often in group discussions. F.D.-P. and R.H. made the figures. F.D.-P., C.D.N. and K.D. wrote the manuscript with input from all authors.

Competing interests

The authors declare no competing interests.

Additional information

Extended data is available for this paper at https://doi.org/10.1038/s41564-019-0579-2.

Supplementary information is available for this paper at https://doi.org/10.1038/s41564-019-0579-2.

Correspondence and requests for materials should be addressed to K.D.

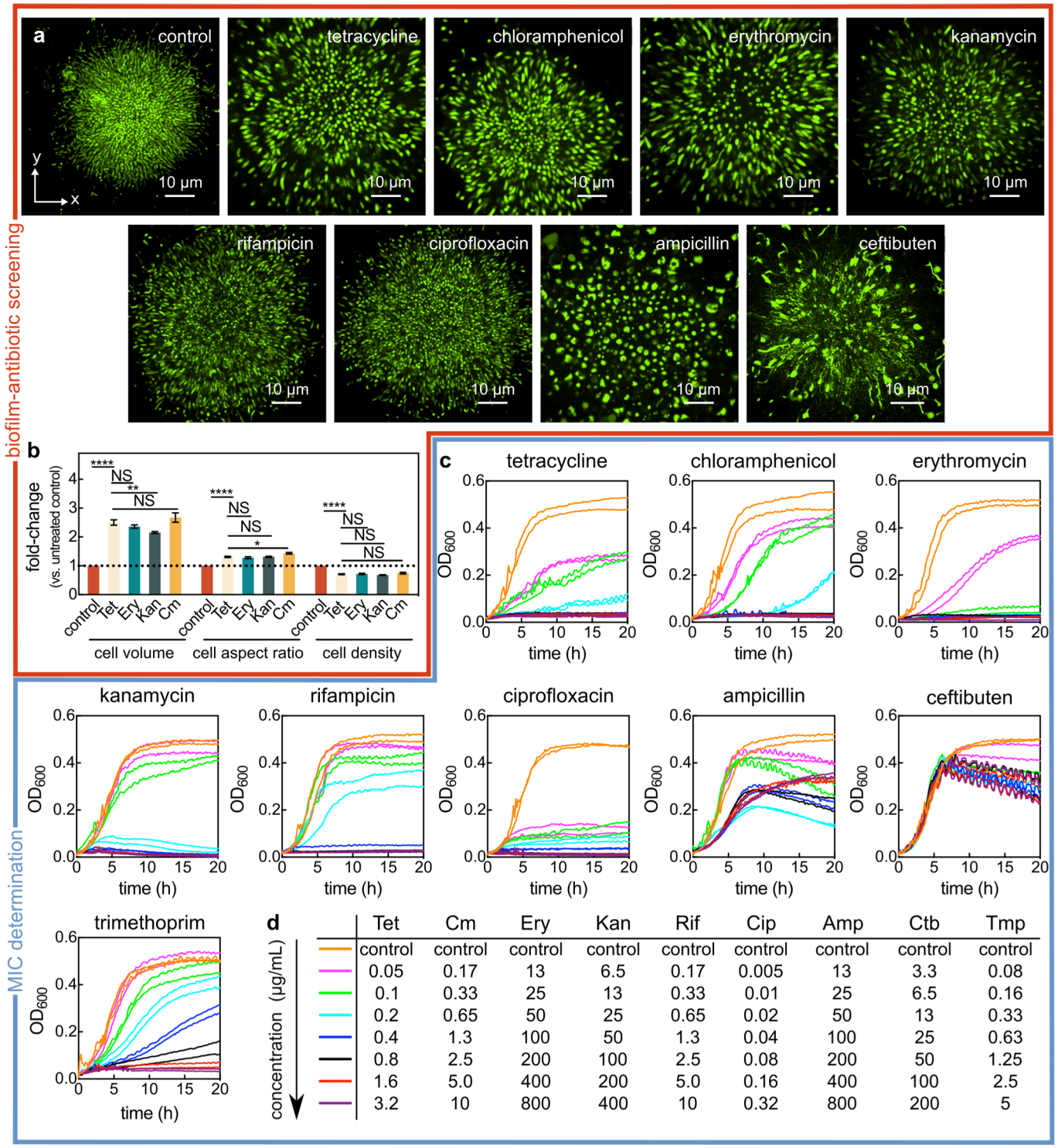

	Tet	Cm	Ery	Kan	Rif	Cip	Amp	Ctb	Tmp
	control	control	control	control	control	control	control	control	control
	0.05	0.17	13	6.5	0.17	0.005	13	3.3	0.08
	0.1	0.33	25	13	0.33	0.01	25	6.5	0.16
	0.2	0.65	50	25	0.65	0.02	50	13	0.33
	0.4	1.3	100	50	1.3	0.04	100	25	0.63
	0.8	2.5	200	100	2.5	0.08	200	50	1.25
	1.6	5.0	400	200	5.0	0.16	400	100	2.5
	3.2	10	800	400	10	0.32	800	200	5

Extended Data Fig. 1 | Screening biofilm architecture after antibiotic exposure and identifying the minimum inhibitory concentration (MIC). (**a**) Confocal *xy*-slices of biofilms exposed to different antibiotics for 24 h and stained with the SYTO 9 nucleic acid dye. The conditions tests were the following: untreated control biofilm, tetracycline (Tet; 3 µg/mL, 8x the MIC), chloramphenicol (Cm; 10 µg/mL, 8x the MIC), erythromycin (Ery; 200 µg/mL, 4x the MIC), kanamycin (Kan; 200 µg/mL, 4x the MIC), rifampicin (Rif; 6 µg/mL, 5x the MIC), ciprofloxacin (Cip; 0.5 µg/mL, 6.3x the MIC), ampicillin (Amp; 400 µg/mL, a concentration at which the cell morphology was significantly modified), and ceftibuten (Ctb; 50 µg/mL, a concentration at which the cell morphology was significantly modified). Images are representative of $n = 3$ independent experiments. (**b**) Fold-change of cell volume, cell aspect ratio, and cell density (calculated as volume fraction) of biofilms treated with different protein synthesis inhibitors for 6 h, relative to untreated biofilms (mean ± SEM, $n = 15$ samples for control, $n = 9$ for Tet, $n = 7$ for Ery, $n = 14$ for Kan, and $n = 8$ for Cm; samples correspond to different biofilms). Statistical significances were calculated using a one-way ANOVA with Bonferroni's correction. Statistically non-significant differences (NS) correspond to $p = 0.93$, 0.51, 0.99, 0.99, 0.99, 0.99, 0.46 (left to right). *, ** and **** indicate $p < 0.05$, $p < 0.01$ and $p < 0.0001$ respectively. (**c**) Batch culture growth curves of wild-type *V. cholerae* N16961 grown in M9 medium supplemented with glucose and with different antibiotic concentrations. Every line corresponds to the average between 2 technical replicates, and each concentration has been tested on 2 separate days (each resulting in one line). For ampicillin and ceftibuten, the MIC determination was not possible from the concentrations tested, due to the lack of cell lysis. (**d**) List of antibiotic concentrations used in panel **c** according to their color-coding.

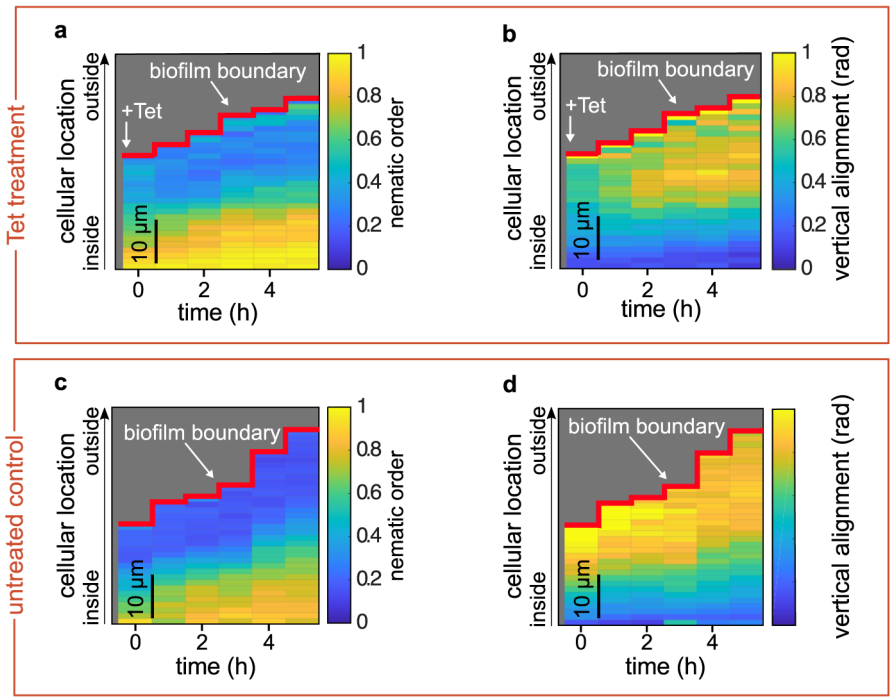

Extended Data Fig. 2 | Nematic order and vertical alignment of cells in biofilms during tetracycline treatment, compared with untreated controls. (**a**, **b**) Spatiotemporal changes of the average nematic order (**a**), or the vertical alignment (**b**), as a function of time and position inside the biofilm during tetracycline treatment. Each pixel in the heatmap is coloured according to the average nematic order (**a**) or vertical alignment (**b**) at a given time and spatial position in the biofilm. (**c**, **d**) Spatiotemporal changes of the average nematic order (**c**), or the vertical alignment (**d**), for control biofilms that were not treated with tetracycline. In these kymograph heatmaps, the pixel values correspond to averages over all cells with similar distances from the surface of the biofilm at a particular time. Heatmaps are representative of $n = 5$ different biofilms.

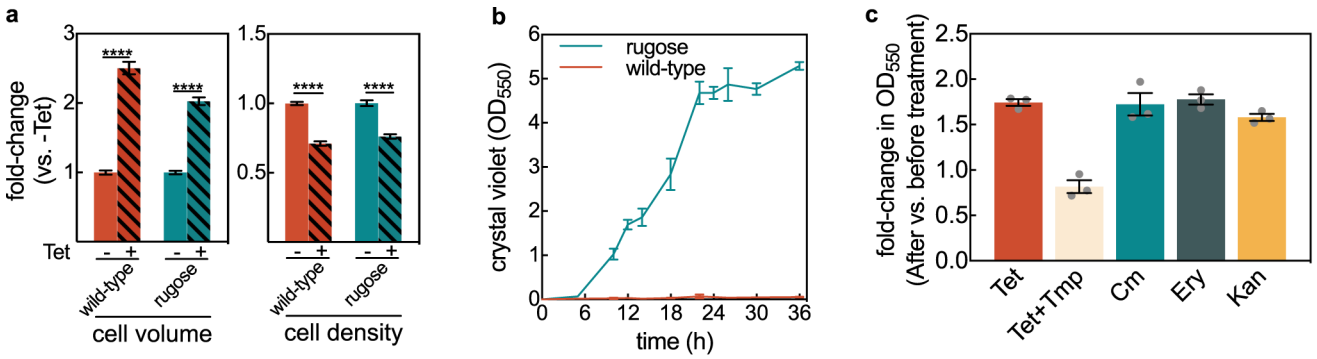

Extended Data Fig. 3 | Effect of tetracycline treatment on biomass measurements using the crystal violet assay. (**a**) Fold-changes for the cell volume and cell density of the wild- type (WT) and the *vpvC*^{W240R} rugose strain (which is a biofilm hyper-producer strain[47]) for tetracycline-treated biofilms in comparison with untreated biofilms, measured in flow chambers using confocal imaging at the single-cell level. Data are shown as mean ± SE, $n = 15, 9, 7, 11$, for WT (-Tet), WT (+Tet), rugose (-Tet), and rugose (+Tet), respectively. Each sample corresponds to an independent biofilm. These results show that the rugose strain also displays similar biofilm architecture responses to Tet treatment. Statistical significances were calculated using a one-way ANOVA with Bonferroni's correction. **** indicates $p < 0.0001$. (**b**) Growth curve of rugose and WT biofilms using the crystal violet assay in 96-well plates; mean ± SD, $n = 3$ independent biological replicates. These results show that only the rugose strain forms substantial biofilms in static 96-well plates. (**c**) Fold-change in biofilm biomass measured by crystal violet absorbance of rugose biofilms, which were grown for 14 h in 96-well plates followed by 6 h treatment with tetracycline (Tet; 3 μg/mL, 8x the MIC), trimethoprim (Tmp; 10 μg/mL, 4x the MIC), chloramphenicol (Cm; 10 μg/mL, 8x the MIC), erythromycin (Ery; 200 μg/mL, 4x the MIC), or kanamycin (Kan; 200 μg/mL, 4x the MIC); mean ± SE, $n = 3$ independent biological replicates. For all experiments, each biological replicate is the average of 8 technical replicates from different wells on the same microtiter plate. The translational inhibitors Tet, Cm, Ery, and Kan show the same qualitative behaviour: an increase in crystal violet biofilm signal after 6 h of antibiotic exposure. Only the Tet+Tmp treatment does not show the increase in crystal violet signal, consistent with Fig. 2g of the main text.

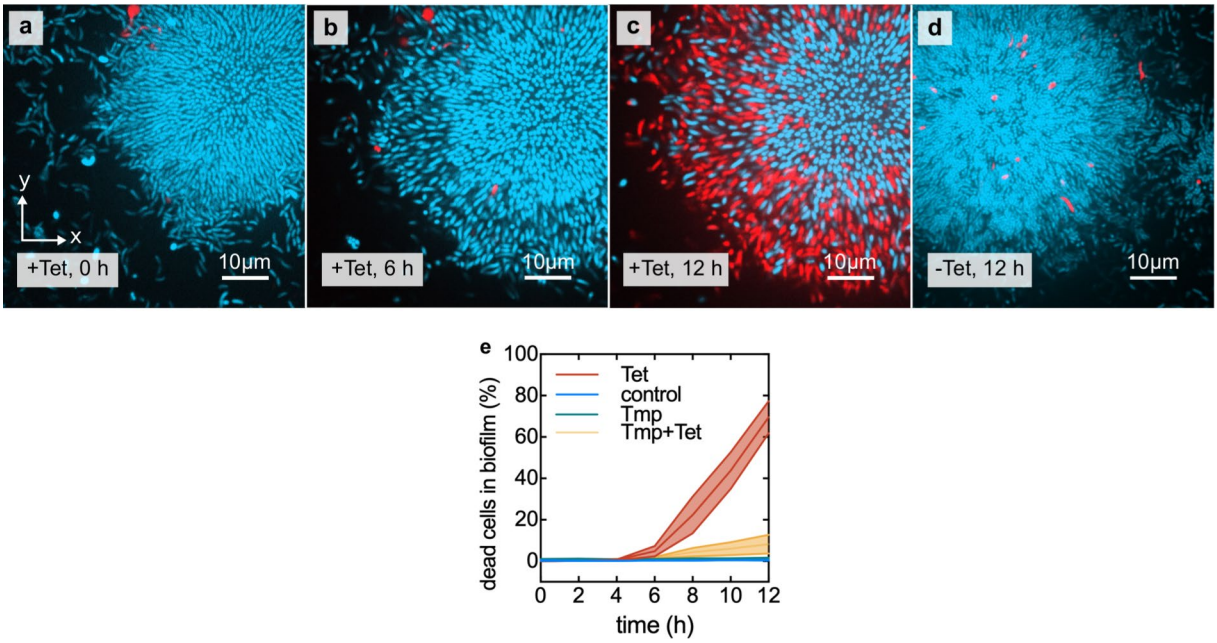

Extended Data Fig. 4 | Increase in cell volume and decrease in cell density precede cell death. (**a**) Confocal *xy*-slices of a biofilm constitutively expressing mTFP1 (shown in cyan), grown in the presence of propidium iodide. Alive cells are only visible in the cyan fluorescent channel, whereas dead cells are also visible in the red fluorescent channel. (**b**) Same biofilm as in panel **a**, now imaged after 6 h of tetracycline (Tet) treatment. (**c**) Same biofilm as in panel **a**, after 12 h of Tet treatment. (**d**) Untreated control biofilm. (**e**) Percentage of dead cells in the biofilm as a function of treatment time. Centre lines correspond to mean and width of the shaded areas around each line correspond to standard errors, $n = 13$ samples for Tet, $n = 9$ for control, $n = 4$ for Tmp, $n = 4$ for Tmp+Tet. Each sample corresponds to a different biofilm.

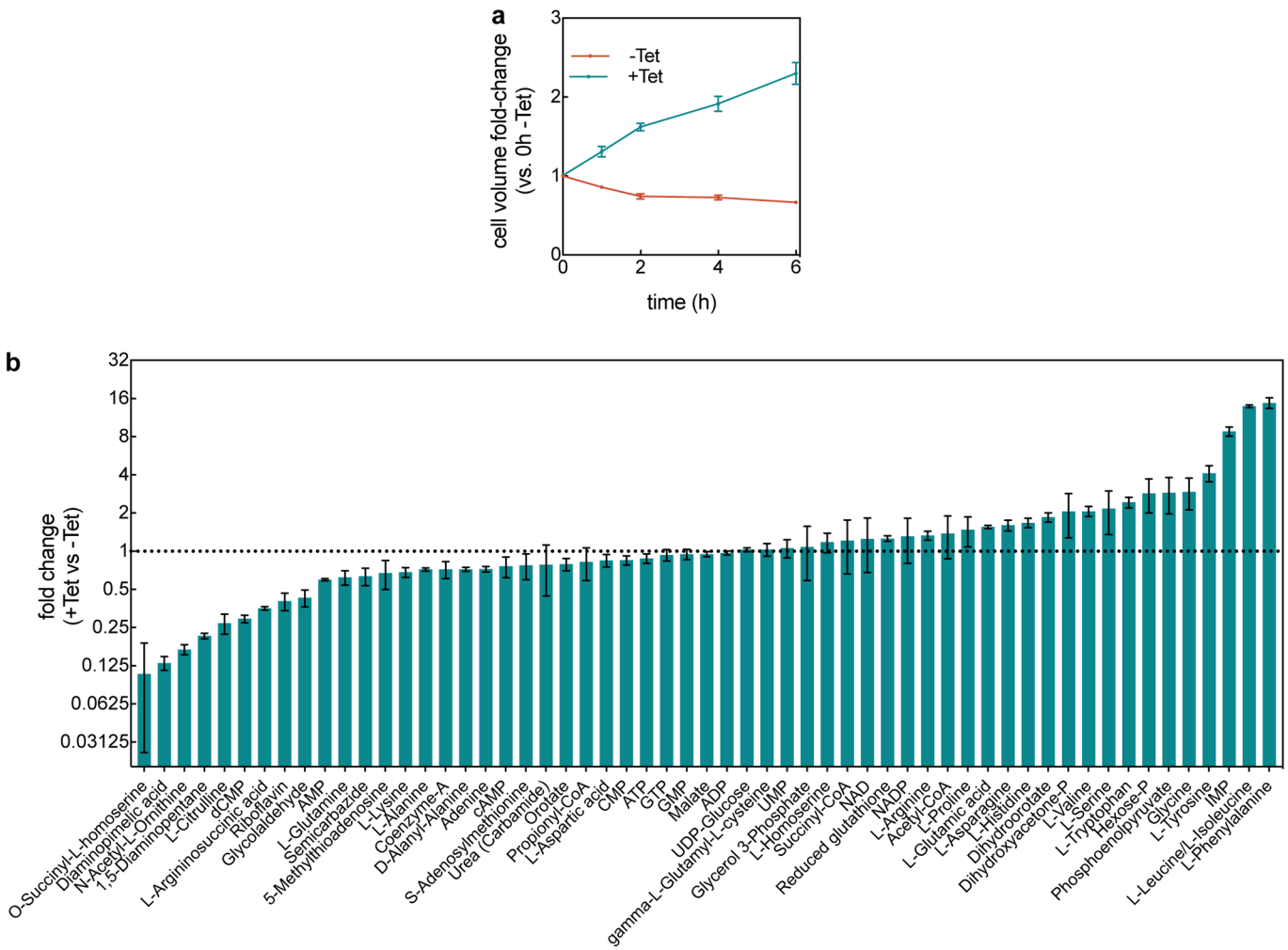

Extended Data Fig. 5 | Changes in cell volume and metabolite levels of planktonic cells during exposure to tetracycline. (**a**) Cell volume fold-change (comparing each time point to the untreated (-Tet) sample at 0 h (mean ± SEM, $n = 5$ independent biological replicates. (**b**) Fold-changes in 57 metabolites after 2 h of Tet treatment in comparison with untreated cells (mean ± SEM, $n = 3$ independent biological replicates).

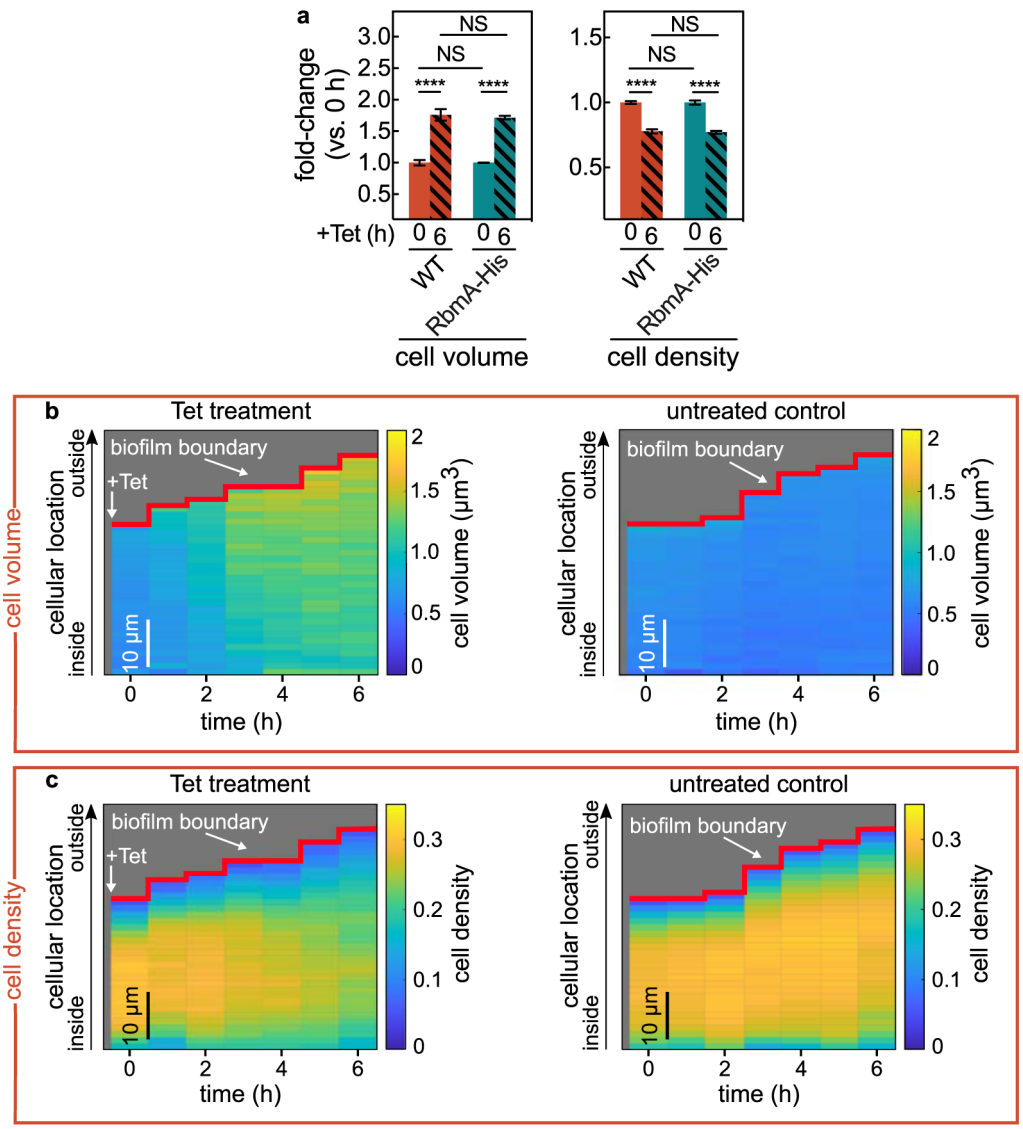

Extended Data Fig. 6 | The RbmA-His strain phenocopies the wild- type strain. (**a**) Fold-change of cell volume and cell density (measured as volume fraction) of wild-type biofilms and biofilms formed by a strain producing His-tagged RbmA (RbmA-His) treated with tetracycline, relative to the biofilms before the treatment. Values are displayed as mean ± SEM ($n = 17$ different biofilms). Statistical significances were calculated using a one-way ANOVA with Bonferroni's correction for multiple comparisons. Statistically non-significant differences are labelled NS, which both correspond to $p = 0.99$. **** indicates $p < 0.0001$. (**b**, **c**) RbmA-His biofilms, shown here, display the same spatiotemporal changes in biofilm architecture as the WT biofilms, for which the corresponding kymograph heatmaps are shown in Fig. 1e–h. Heatmaps show the changes of the average cell volume (**b**) and cell density (**c**) as a function of time and spatial location during tetracycline treatment inside the RbmA- His biofilms. Panels on the left correspond to Tet treatment and panels on the right correspond to untreated control conditions. Each pixel in these kymograph heatmaps is coloured according to the average cell volume or cell density at a given time and spatial position in the biofilm. Cell volumes and cell density volume fraction values are averaged over all cells with similar distances from the surface of the biofilm. The RbmA-His strain was grown and imaged using antibodies as described in the methods section. Heatmaps are representative of $n = 5$ different biofilms.

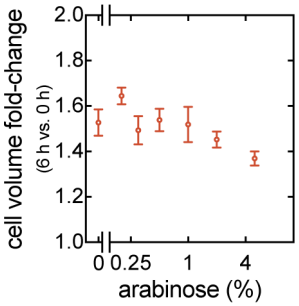

Extended Data Fig. 7 | Antibiotic-induced cell volume increase is independent of RbmA concentration. Cell volume fold-change (comparing 6 h and 0 h of Tet treatment) in biofilms of a Δ*rbmA* strain carrying the P_{BAD}:*rbmA* construct, measured as a function of arabinose concentration (mean ± SEM, $n = 7, 12, 13, 17, 10, 18, 14$ samples for arabinose concentrations of 0%, 0.2%, 0.3%, 0.5%, 1%, 2%, and 5% respectively). Each sample corresponds to a different biofilm.

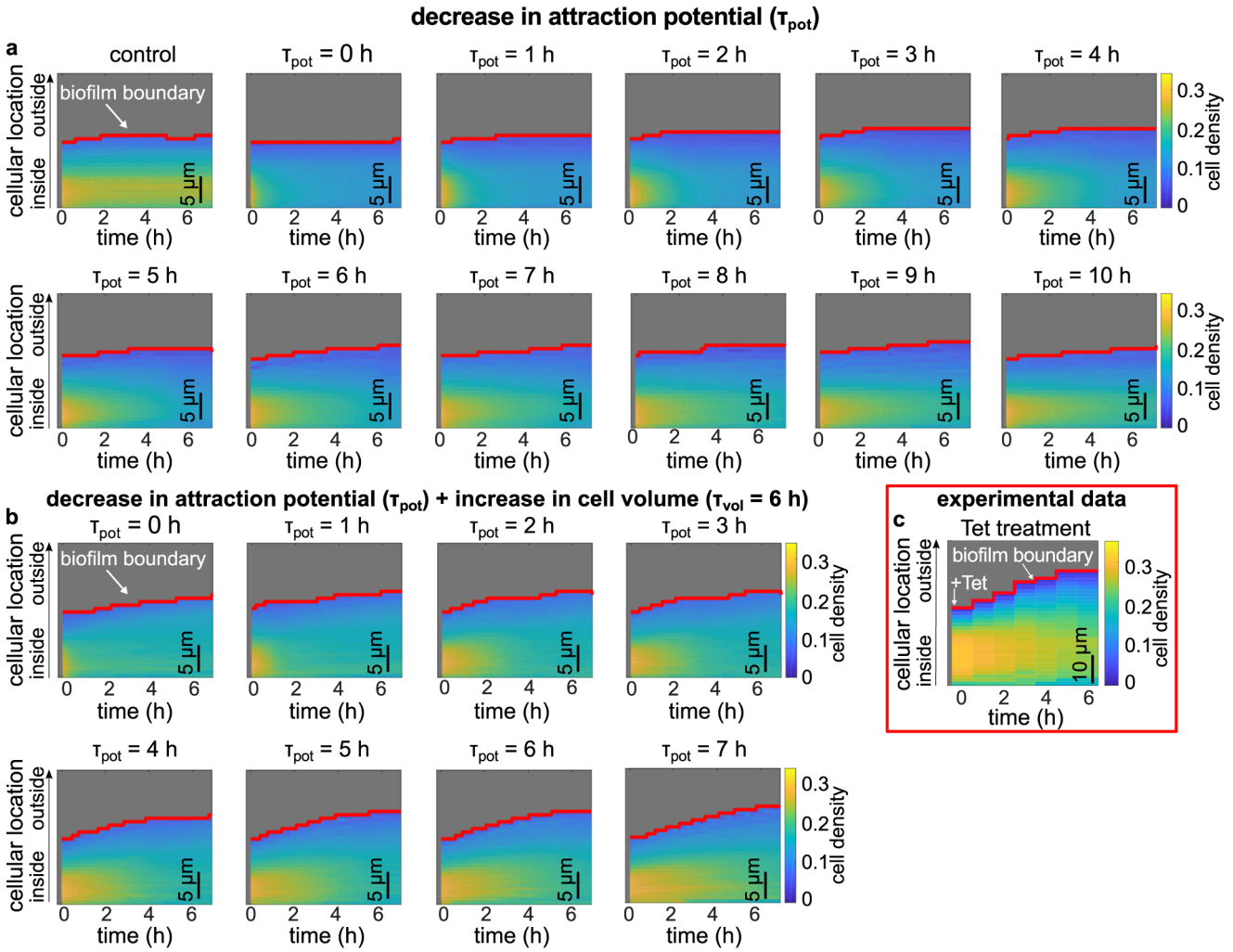

Extended Data Fig. 8 | Simulated biofilms were subjected to a decrease in cell-cell attraction and an increase in cell volume, revealing the contribution of each effect to the antibiotic-induced biofilm architecture changes. Biofilm growth was simulated as described in the methods section until the biofilm size reached 1,000 cells, corresponding to the 0 h time point in the heatmaps in this figure. For these 1,000-cell biofilms, tetracycline treatment was simulated by decreasing the attraction potential, or by increasing the cell volume, or by both effects together. (**a**) Kymograph heatmaps of simulated 1,000-cells biofilms subject to a linear decrease in cell-cell attraction over the course of different times τ_{pot}. The value of τ_{pot} corresponds to the time for the cell-cell attraction potential to decrease to zero, starting from the value used to simulate biofilm growth. If the attraction potential is set to zero immediately (corresponding to $\tau_{pot} = 0$), the resulting biofilm dynamics do not closely resemble the experiments, indicating that the cell-cell attraction decreases over an extended period of time. The control kymograph heatmap corresponds to biofilms were neither the attraction potential or the cell volume were changed. Each heatmap is the average of $n = 3$ simulations. (**b**) Heatmaps of simulated 1,000-cells biofilms that were subjected to a decrease in cell-cell attraction over different times (τ_{pot}) and simultaneously subjected to a linear increase in cell volume over 6 h ($\tau_{vol} = 6$ h). Each heatmap is the average of $n = 3$ simulations. In Fig. 3h of the main text, a kymograph heatmap is shown for simulations in which only the cell volume is linearly increased with a time scale $\tau_{vol} = 6$ h, according to the experimentally determined single-cell volume growth rate during Tet-treatment. (**c**) Experimental changes of the average cell density as a function of space and time during tetracycline treatment inside the biofilm as shown in Fig. 1g, reproduced here for convenience. Heatmap in panel **c** is a representative of $n = 5$ different biofilms.

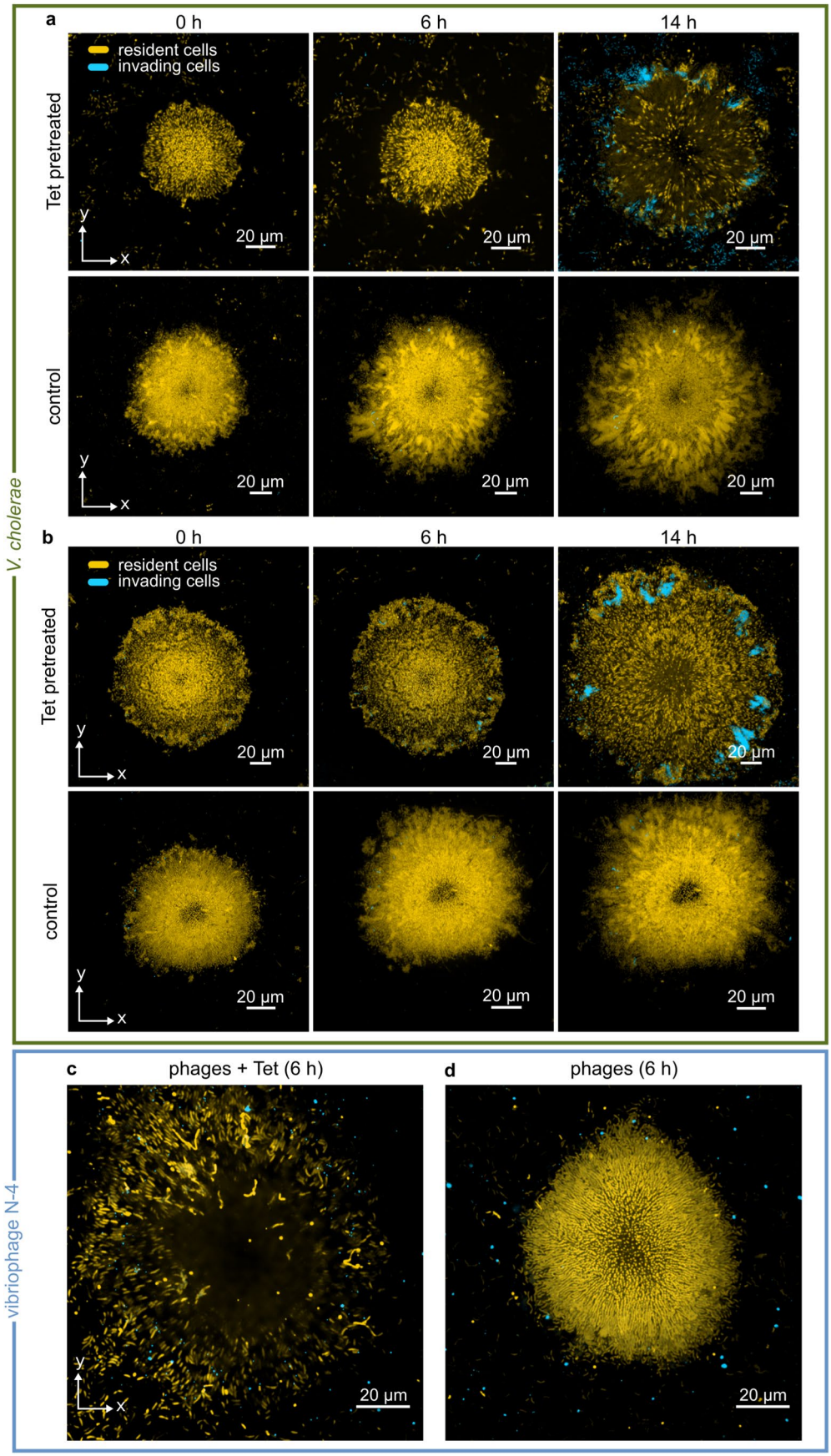

Extended Data Fig. 9 | see figure caption on next page.

Extended Data Fig. 9 | Tetracycline-treated *V. cholerae* biofilms are susceptible to colonization and population invasion by an isogenic strain and by bacteriophages. (**a**-**b**) Each of the two panels shows an independent replica experiment of a tetracycline-treated *V. cholerae* biofilm colonized by an isogenic strain, which is expressing a different fluorescent protein. Resident biofilms constitutively express mKOκ (cells shown in yellow), invaders constitutively express sfGFP (cells shown in cyan). Images correspond to confocal *xy*-slices, acquired 2 μm above the substrate. The resident biofilm underwent tetracycline (Tet) treatment for 6 h or control treatment (medium without Tet), followed by 2 h exposure to invader cells. Following exposure to invader cells, the medium was exchanged to fresh, sterile medium and the imaging was started (labelled as the 0 h time point here). A third independent replica experiment is shown in Fig. 4a, b of the main text. (**c**) Confocal *xy*-slice of a resident *V. cholerae* WT biofilm, expressing mKOκ constitutively (cells shown in yellow), imaged directly above the glass substrate. The resident biofilm underwent exposure to tetracycline (Tet) and fluorescently labelled vibriophage N-4 virions (visible as cyan spots) for 6 h. During 6 h of Tet-treatment cell death is negligible, as shown in Extended Data Fig. 4. (**d**) Confocal *xy*- slice of control biofilm (not treated with tetracycline) exposed to vibriophage N-4 virions for 6 h. Images are representative of $n = 5$ different biofilms.

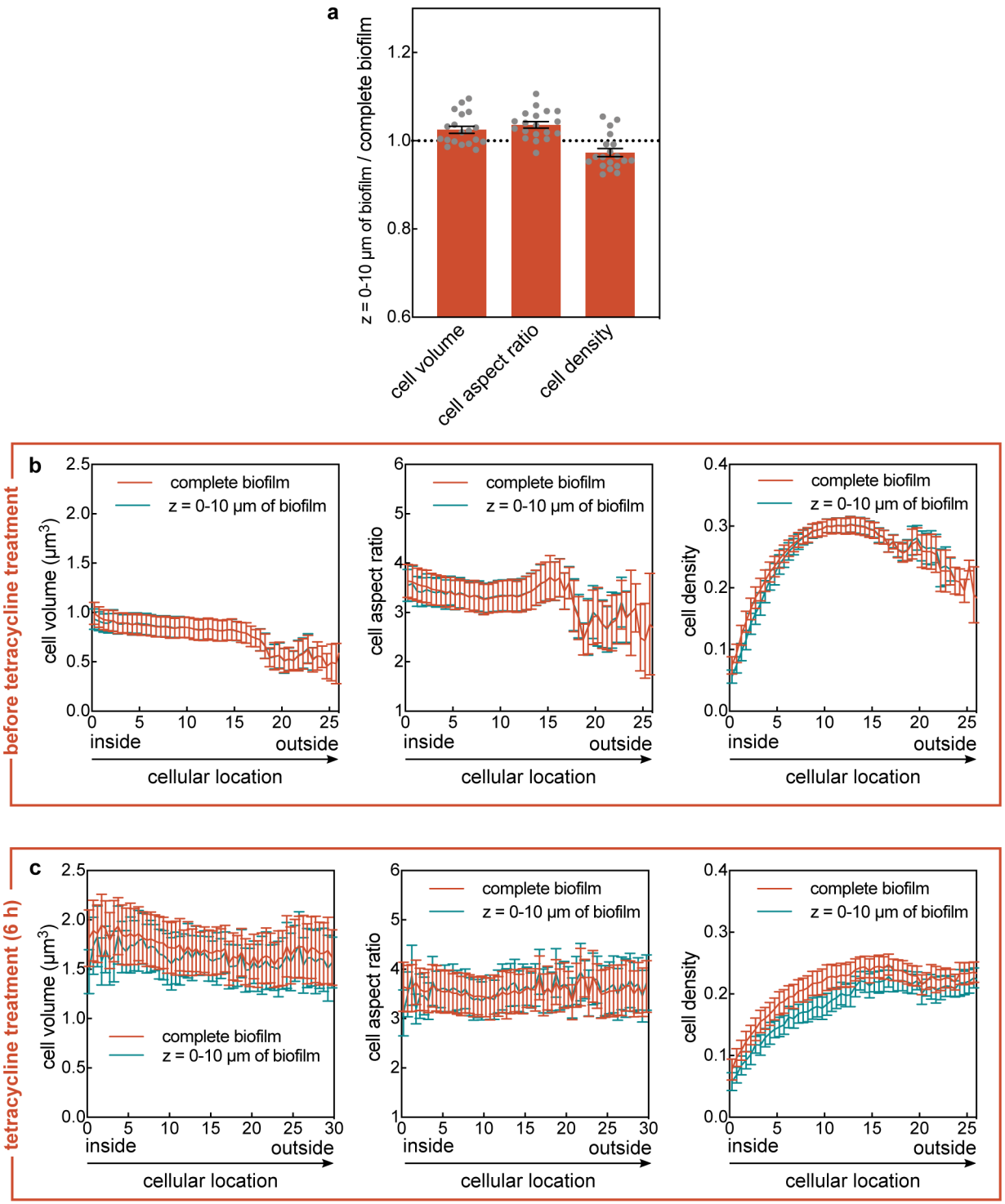

Extended Data Fig. 10 | Biofilm architecture in the lower part of the biofilm is representative of the whole biofilm. (**a**) Comparison between the cell volume, cell aspect ratio, and cell density (measured as volume fraction) between the lower part of the biofilm and the whole biofilm. The ratio of these biofilm architecture parameters was calculated using the mean value of these parameters in the part of the biofilm that is bounded by the $z = 0$ µm and $z = 10$ µm planes, and the mean value of these parameters in the whole biofilm (mean ± SEM, $n = 19$ different biofilms). (**b**, **c**) Cell volume, cellular aspect ratio, and cell density before tetracycline treatment (panel **b**) or after 6 hours of tetracycline treatment (panel **c**) as measured for complete biofilm volumes, or for the cells located in the biofilm volume bounded by the $z = 0$ µm and $z = 10$ µm planes (mean ± SD, $n = 8$ samples in panel **b** and $n = 5$ samples in panel **c**; each sample corresponds to a different biofilm). The cellular location was measured as the shortest distance of each cell to the interface between the biofilm and the liquid growth medium. This interface is termed "biofilm boundary" in this manuscript. For the experiments in this figure, biofilms were stained with the nucleic acid dye SYTO 9 prior to imaging. The cell volume, aspect ratio, and cell density were nearly identical between the whole biofilm and the bottom-most 10 µm of the biofilms.

nature research

Corresponding author(s): Knut Drescher

Reporting Summary

Nature Research wishes to improve the reproducibility of the work that we publish. This form provides structure for consistency and transparency in reporting. For further information on Nature Research policies, see Authors & Referees and the Editorial Policy Checklist.

Statistical parameters

When statistical analyses are reported, confirm that the following items are present in the relevant location (e.g. figure legend, table legend, main text, or Methods section).

n/a	Confirmed	
☐	☒	The exact sample size (*n*) for each experimental group/condition, given as a discrete number and unit of measurement
☐	☒	An indication of whether measurements were taken from distinct samples or whether the same sample was measured repeatedly
☐	☒	The statistical test(s) used AND whether they are one- or two-sided *Only common tests should be described solely by name; describe more complex techniques in the Methods section.*
☐	☒	A description of all covariates tested
☒	☐	A description of any assumptions or corrections, such as tests of normality and adjustment for multiple comparisons
☐	☒	A full description of the statistics including central tendency (e.g. means) or other basic estimates (e.g. regression coefficient) AND variation (e.g. standard deviation) or associated estimates of uncertainty (e.g. confidence intervals)
☐	☒	For null hypothesis testing, the test statistic (e.g. *F*, *t*, *r*) with confidence intervals, effect sizes, degrees of freedom and *P* value noted *Give P values as exact values whenever suitable.*
☒	☐	For Bayesian analysis, information on the choice of priors and Markov chain Monte Carlo settings
☒	☐	For hierarchical and complex designs, identification of the appropriate level for tests and full reporting of outcomes
☒	☐	Estimates of effect sizes (e.g. Cohen's *d*, Pearson's *r*), indicating how they were calculated
☐	☒	Clearly defined error bars *State explicitly what error bars represent (e.g. SD, SE, CI)*

Our web collection on statistics for biologists may be useful.

Software and code

Policy information about availability of computer code

Data collection	Nikon NIS Elements Advanced Research 4.5 software was used to control microscopes.
Data analysis	Matlab (version R2018b) was used to analyze data. A detailed description of the analysis is provided in the Materials and Methods section.

For manuscripts utilizing custom algorithms or software that are central to the research but not yet described in published literature, software must be made available to editors/reviewers upon request. We strongly encourage code deposition in a community repository (e.g. GitHub). See the Nature Research guidelines for submitting code & software for further information.

Data

Policy information about availability of data

All manuscripts must include a data availability statement. This statement should provide the following information, where applicable:

- Accession codes, unique identifiers, or web links for publicly available datasets
- A list of figures that have associated raw data
- A description of any restrictions on data availability

Provide your data availability statement here.

Field-specific reporting

Please select the best fit for your research. If you are not sure, read the appropriate sections before making your selection.

☒ Life sciences ☐ Behavioural & social sciences ☐ Ecological, evolutionary & environmental sciences

For a reference copy of the document with all sections, see nature.com/authors/policies/ReportingSummary-flat.pdf

Life sciences study design

All studies must disclose on these points even when the disclosure is negative.

Sample size	Each of the n replicates of each experiment is the average of hundreds to thousands of bacterial cells as a sample size. Each experiment was replicated independently at least 3 times, but usually n>3. The n for each experiment is indicated in each figure.
Data exclusions	No data were excluded.
Replication	Each experiment was replicated n times (and n is given in each figure for each experiment). Although the exact quantitative results differ between replicates, the qualitative results were the same, so that it is reasonable to state that the "replication was successful".
Randomization	There were many bacterial cells within each of the n replicates. Because of the large sample size for each replicate, a representative number of samples were collected for each replicate. There was no allocation of samples into experimental groups, beyond conducting independent biological replicates.
Blinding	Blinding of group allocation is irrelevant to our data analysis, because there was no allocation to experimental groups, beyond collecting n replicates, all of which were analyzed by software equally.

Reporting for specific materials, systems and methods

Materials & experimental systems

n/a	Involved in the study
☒	☐ Unique biological materials
☐	☒ Antibodies
☒	☐ Eukaryotic cell lines
☒	☐ Palaeontology
☒	☐ Animals and other organisms
☒	☐ Human research participants

Methods

n/a	Involved in the study
☒	☐ ChIP-seq
☒	☐ Flow cytometry
☒	☐ MRI-based neuroimaging

Antibodies

Antibodies used	Commercial Antibodies were used as described in detail (including part numbers) in the Materials and Methods section.
Validation	Validation: Biofilms grown from strains that do not contain the 6xHis modification to RbmA did not show any antibody signal.